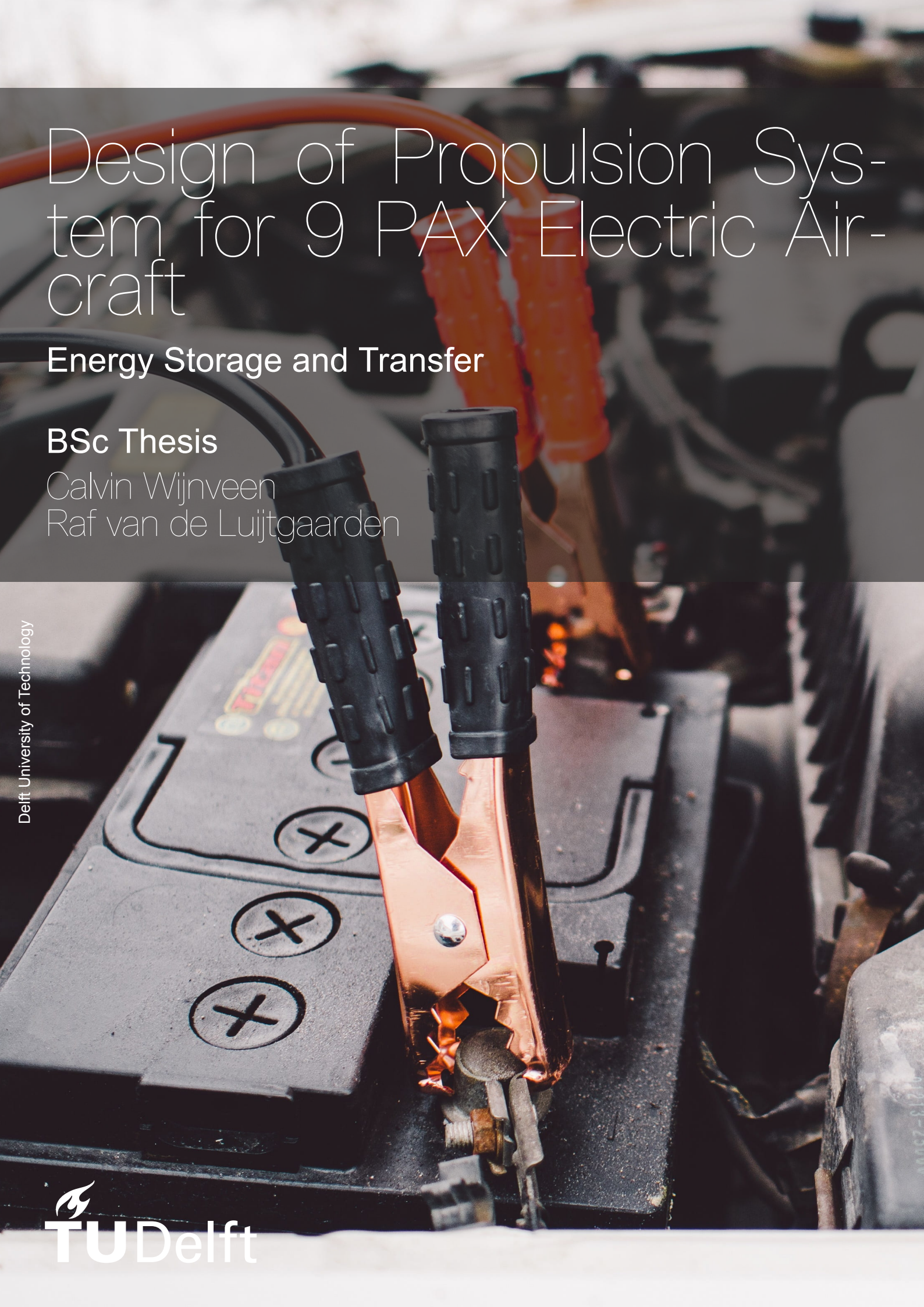

Design of Propulsion System for 9 PAX Electric Aircraft

Energy Storage and Transfer

BSc Thesis

Calvin Wijnveen
Raf van de Luijtgaarden

Delft University of Technology

TU Delft

Design of Propulsion System for 9 PAX Electric Aircraft

Energy Storage and Transfer

by

Calvin Wijnveen
Raf van de Luijtgaarden

to obtain the degree of Bachelor of Electrical Engineering
at the Delft University of Technology,
to be defended publicly on Thursday June 23, 2022 at 09:00 AM.

Student number:	5064449	(Calvin Wijnveen)
	5159415	(Raf van de Luijtgaarden)
Project duration:	April 19, 2022 – June 24, 2022	
Head Supervisor:	Gauthaum R. C. Mouli	
Supervisor	Jianning Dong	
Supervisor	Mohamad G. Niasar	

TU Delft

Abstract

In 2018 it was estimated that the aviation industry produced approximately 1.04 billion tons of CO2. This was an estimated 2.5% of the total CO2 emitted that year. In order to slow down global warming, big changes need to be made to the transportation industry. This change has already begun with commercialization of electric cars. The next step is clear: fully electric, zero emission air crafts. This projects goal is design a high power propulsion system for an electric aircraft set to launch in the year 2040. This project attempts at predicting how this propulsion system might look like, specifically the electrical architecture. This thesis looks at the battery energy storage system, the wiring system and how to deal with high-voltage phenomena at low pressure. Several simulations are performed to justify design choices and give a visual representation of the different design options.

Preface

In the final year of the Bachelor of Electrical Engineering, we as students are required to participate in a group project proposed by supervisors. Our proposed project was based on the *IEEE/AIAA ITEC+EATS Design Competition of a High-Voltage/ High Power Distribution Propulsion System for Zero Emission Aircraft*. In the project it is required to deliver a design of the electrical propulsion system based on the technology available in 2038. In the reports, we complete the design assignment by making critical technical choices on various components and subsystems. The state of the art of relevant technologies and their evolving trend towards 2038 have been summarized from available research papers, technical reports and product data sheets. The technical choices have been made following the design guidelines, requirements and restrictions set by the competition. Through looking at these guidelines we could split the tasks into 3 subgroups: electrical power distribution and e-motors, safety considerations and power converters, and energy storage and transfer. Each subgroup contributed a part of the design so that all parts could make one final design which described the high power distribution system. Based on the competition guidelines we could split the workload up almost equally between the 3 subgroups. Our group specifically focused on how we would provide energy for the electric aircraft and how this energy was transported throughout its respective systems.

Calvin Wijnveen
Raf van de Luijtgaarden
Delft, June 2022

Contents

1 Introduction

In our ever-changing world where an increasing amount of people are born every day, the topic of climate change gets progressively more important and urgent. The last century has brought an incredible amount of inventions that improve quality of life, including worldwide travel opportunities. Commercial aviation emitted 2.4% of all CO_2 in 2018, with more becoming inevitable as more people get access to flying. With these considerations in mind, no-emission flying is the next benchmark in a greener and more sustainable future. High capacity batteries charged by renewable energy sources are already flooding the market in electric cars and in some cases, small airplanes. Standard Lithium-ion (Li-ion) batteries used today are limited by their low energy density, calling for research in other battery compounds. Lithium-Sulfur (Li-S) batteries are a recent technology with a promising future to bring full-electric flying to the world. More promising advances regarding this battery technology, power coupling, safety, propulsion systems and weight reduction enable research today, for the future.

1.1. Thesis Objective

The objective of this thesis is to design an electric aircraft for 2038 by the requirements given in a competition by a collaboration between the Institute of Electrical and Electronics Engineers (IEEE) and American Institute of Aeronautics and Astronautics (AIAA), which can be found later in this thesis. This problem is tackled by a group of 6 students and a division in three subgroups has been made to tackle different aspects of the challenge:

- **Electric Motors and Power Distribution**
- **Energy Storage and Transfer**
- **Power Converters and Safety Considerations**

In this thesis, the energy storage and transfer of this all-electric aircraft will be presented. This includes specifications regarding the cell technology, wiring materials and components as well as the safety measures taken to mitigate some problems in wiring and battery that occur in high power systems. Each of these topics will be backed by information and weight estimations to keep the weight of this plane as low as possible while ensuring a reliable and functioning design. Because the challenge focuses on a design for 2038, extrapolation and reasoning will be a common theme throughout the thesis to back up the choices made.
Next, a summary of the thesis structure is given to present the research done for this project.

1.2. Thesis Structure

In Chapter 2, the program of requirements is presented along with goals that need to be fulfilled. Then, in Chapter 3, a deep dive is done into the battery system design ranging from the cell technology to the properties and architecture and safety considerations regarding thermal runaway, as well as a look into a battery management system. Chapter 4 provides research regarding the wiring system of the electric aircraft, from materials to weight, temperature and connectors used throughout the aircraft. Following

these discussions, Chapter 5 delves into the risks that come with high-voltage operations and provides methods and systems to mitigate partial discharges and arcing in the wires. Chapter 6 reflects on the achieved work along with a discussion. Finally, Chapter 7 concludes the thesis and lays out options for future work regarding the topics discussed throughout.

2

Program of Requirements

2.1. Intergroup Requirements

This project called for the design of a propulsion system suited for an all electric aircraft. In order for the design to be a viable option, it must fit specific requirements. The propulsion system is broken down into 7 categories that were distributed amongst the researchers participating in this project. Each group of two researchers had to keep some general requirements in mind that would provide constraints to the design. These requirements are listed below.

- Minimum cruise speed of 500 km/h, target cruise speed of 550 km/h or greater.
- Capable of flying in known icing conditions (deicing of the wings and other systems).
- Meets applicable certification rules in FAA 14 CFR Part 13.
- Year of entry is 2038. All technology should be taken as if it were 2038.
- The MTOW (maximum take-off weight) is 5650 kg.
- The payload is 1000 kg, which includes the 9 PAX, 1 crew member and all luggage.
- The expected propulsion system weight is 1650 kg, however, if it exceeds this amount then the payload capability is reduced.
- Total embedded power of 2 MW.
- 4 electric motors, 2 motors per wing.
- The airplane mission range is 260 km which includes a 50 km backup reserve.
- Altitude ceiling of 9 km.
- Requested power for the climb to cruise altitude: 1150 kW.
- Cruise and descent duration of 28 minutes with an average requested power of 515 kW.

2.2. Intragroup Requirements

The specific requirements for the content of this thesis is more focused towards the energy requirements and the safety of this electrical distribution with respect to high-voltage phenomena. The requirements are split up into the main sections covered in this paper.

Battery Energy Storage System Requirements

- The cell technology used should be technology that will be available in 2038.
- Estimation of the total weight of the battery energy storage system.
- Energy density and power density at the battery level should be calculated.
- A justified explanation of the battery distribution in the aircraft.
- Methods for thermal runaway mitigation.

Wiring System Requirements

- How to choose a conductor size.
- A hypothesis of temperature in the cable.
- What connectors are used in the aircraft.

High-Voltage Requirements

- How are partial discharges prevented.
- Sizing rules for insulation with lower pressure in mind.
- How is series and parallel arcing prevented.
- Short-circuit current estimation.
- Explanation of components used for arc mitigation.

3

Energy Storage: Battery System

For the electric aircraft to be powered, a battery energy storage system (BESS) is used to supply electrical energy to all on-board electrical components, including lighting, pressurisation and air-conditioning to defrosting the wings and driving the motors to fly the plane itself. This BESS will be charged and discharged between flights, making it an environmentally-friendly way of traveling through the air. In aviation, weight is of utmost importance. A light, yet energy-dense BESS design is crucial for an all-electric airplane. This chapter will discuss all aspects regarding the BESS: the cell technology analysis, the properties and architecture and the safety considerations needed to ensure a safe and powerful battery.

3.1. Cell Technology

For the energy storage system, batteries with a high cell volume will be used. In this section, several cell technologies/chemistries will be presented along with several advantages and disadvantages, finishing with a discussion about the chosen technology for the final design.

3.1.1. Lithium-ion Batteries

In the last couple of decades, Li-ion batteries have been a go-to choice for many applications. With their high energy density and long lifetime they have taken over the battery market in many applications going from phones, laptops, cameras, electric tools and most importantly for this thesis, electric vehicles. Nowadays, if a device can be recharged, it is most likely powered by a Li-ion battery.

The popularity and high use of these batteries comes from their great performance on several aspects:

- Energy density
- Low self-discharge rate
- High cell voltage
- Long lifespan
- No maintenance
- Relatively cheap
- Variety of types

Three of these important features considered for an electric plane are the energy density, lifespan and the cell voltage.
A plane has high power demands throughout a flight so a significant amount of energy needs to be stored to supply those demands. The energy density of a material gives information about the amount of energy in J (Joule) or Wh (watt-hour) that can be stored per liter or per kilogram. For a Li-ion battery, this energy density ranges from 100-265 Wh/kg depending on the cell variety.
The lifespan of a battery is measured in cycles, where one cycle means a full charge and discharge of the battery. For Li-ion, these cycles vary from 400-1200 cycles, meaning that the plane battery could

be fully charged and discharged more than a thousand times during its lifetime before needing replacement.
Lastly, due to the high power demands in the plane, multiple cells have to be used in series and parallel to get the desired power output. For Li-ion, the cell voltage is around 3.6 V, meaning that fewer cells need to be used compared to lower-voltage cells, cutting costs and risk of faults.

Li-ion batteries also have some disadvantages regarding safety and cost. While stated that the price of these batteries is relatively cheap, it still clocks in at around $ 132/kWh, making it a costly contender for this project. Additionally, this plane aims to be as environmentally-friendly as possible, which is difficult to achieve with Li-ion batteries, as both nickel and cobalt are used in their manufacturing. These materials are finite and are getting more laborious to come by due to their scarcity and the popularity of the batteries.
In terms of safety, a protection management system is needed for Li-ion batteries, as it has problems with ageing and thermal runaway, which is discussed in Section 3.3 of this chapter.
Due to hazards like fire and explosions, this management system is of utmost important to ensure safety. With planes, factors such as high temperature swings, pressure changes and vibrations make this system more complicated.

An estimation of the total energy usage of the plane during a flight comes at around 450-500 kWh (derived in Section 3.2.1). If Li-ion would be used, which in a excellent cell type has 260 W/kg of energy, a weight of 500 kWh/ 260 W/kg = 1923 kg for the battery alone would be needed to fly this plane. This value would only increase as safety measures and efficiency has yet to be accounted for. Weight is a crucial factor in designing a plane, therefore Li-ion will not be used as it is simply too heavy.

3.1.2. Lithium-air Batteries

Lithium-air batteries are an upcoming technology that makes use of oxygen and lithium. There are two main types, namely the non-aqueous and aqueous battery. Aqueous means that the electrolyte is in water. The theoretical energy densities of these technologies range from 5000 - 11000 Wh/kg [1] depending on the type used. This is almost as much as gasoline, which has an energy density of 12700 Wh/kg. Comparing these densities to the theoretical Li-ion density of 387 Wh/kg, it can be seen that its 13-28 times more energy dense than Li-ion, making it an incredibly powerful and viable technology weight-wise for this project.
However, as mentioned before, the technology is still in its infant state in terms of research and development and will take many years to research the problems and hurdles for this battery type. The biggest hurdles to tackle include [2]:

1. **Poor rate capability**:
   The inability of the cells to deliver the required power.
2. **High overvoltage while charging**:
   Leads to inefficient charging of the battery.
3. **Electrolyte and carbon decomposition**:
   Fast decomposition leads to a low cycle life.
4. **Anode reactivity**:
   If the anode material is too reactive, serious safety threats are possible.

Although the future is very promising, these hurdles are still years if not decades away to being fully tackled, opening the way for commercially available Li-air batteries and vehicles powered by them [3] [4]. Therefore, this type of battery will not be used in this project.

3.1.3. Solid-state Batteries

Solid-state batteries use a solid electrolyte instead of a liquid one, giving room for higher energy densities. There are many solids that can be considered for these batteries to increase capacity and performance. Compared to a Li-ion battery, it has a higher energy storage, weighs less, has a significantly lower risk of failures and fires and can handle higher temperatures [5]. On the other side, they are more expensive to produce and are slower in charging/discharging due to the high resistances at the electrode-electrolyte interface [6]. However, this technology is still in an early development stage,

giving insufficient amount of information to conclude or make reasonable predictions for the future and will thus not be used in this project.

3.1.4. Lithium-sulfur Batteries

Li-S batteries are another choice in the Lithium family adopting different anode and cathode materials with lithium and sulfur, respectively. Consequently, their risk factor becomes significantly lower than those of Li-ion batteries. However, thermal runaway is still an issue with these batteries and therefore monitoring will be necessary.
What makes these batteries attractive is the fact that they use sulfur instead of nickel and cobalt like Li-ion. Sulfur, unlike the aforementioned materials, is abundant over the whole world and is easily acquirable without extensive mining. Economically that makes the batteries cheaper than Li-ion and would decrease in price further in the future. The theoretical energy density of Li-S batteries is 2567 Wh/kg, making it 6.6 times more energy-dense than Li-ion. This technology is still fairly young, but a lot of research has been done and the future is looking very promising. A company called OXIS Energy [7] already powered an FAA approved electric plane designed by Texas Aircraft Manufacturing with their Li-S batteries in 2020 [8], showing that the technology can already be used in aviation. After further research into their future plans, the battery used in this project would be sourced from their technology. Extrapolating their energy density road map, a battery density of around 600-650 Wh/kg is achievable in 2038, which can be seen in Figure 3.1. Therefore, considering the mentioned advantages and future insight, this technology will be used in this energy system. Data, analysis and discussion about the battery design and its properties is done in the next section.

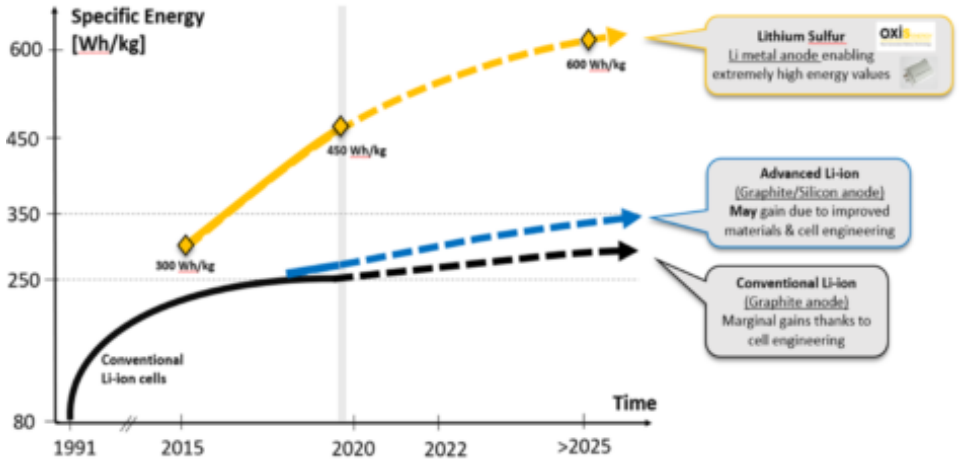

Figure 3.1: OXIS Energy's road map for lithium-sulfur cells gravimetric energy density [7]

OXIS currently has two types of ultra light cells: the high power cell which is suitable for aviation and electric vehicles, and the aeronautical type which is suitable for aeronautical, defence and maritime applications. In their project to supply an electric plane with energy, OXIS proposed the use of the high power cell with gravimetric energy density of 400 Wh/kg. Using this data a sound estimation can be made for what the cells will look like in the future, which can be seen in Table 3.1.

Cell Type	High Power	High Energy	Project Cell
Nominal Voltage (V)	2.1	2.1	2.1
Typical Capacity (Ah)	19±0.5	14.7±0.5	42
C-Rating	6	2	8
Cell Weight (g)	141±2	85±2	138
Energy Density (Wh/kg)	300±5	400±10	650

Table 3.1: Current cell technology and assumed cell technology extrapolated to 2038 based on Figure 3.1 [7].

3.2. Battery Properties & Architecture

At its core, a battery is made up of cells which is what stores chemical potential energy. This chemical potential energy is converted to electrical energy when the two electrodes within a cell are connected. These cells produce a potential difference which is what gives a battery its voltage level. For a single lithium-sulfur cell this nominal voltage is 2.1 V as stated in Table 3.1. This means that in order for a battery to produce a voltage higher than 2.1 volts, these cells should be cascaded in series. Each series cell adds another 2.1 volts to the output of the battery. This means that if one wanted to produce a voltage of 1.5 kV then at least 715 cells with nominal voltage of 2.1 should be connected in series [9]. A cell has a peak C-rating which is a measure of how fast a battery can discharge its total capacity. A C-rating of 1 means that it can produce a current of magnitude equal to its charge capacity [9]. If a single cell cannot produce the desired current that the power system demands then cells should be connected in parallel. For example, if a battery is made up of cells with typical capacities of 42 Ah and peak C-rating of 8 then, in order to produce a current of 667 amps at, at least 2 cells should be connected in parallel. When connecting cells in parallel it is very important that the voltage in the cells is regulated since if there is a voltage mismatch between two cells in parallel it could lead to a short circuit and in some cases thermal runaway (this will be discussed in Section 3.3. This cell voltage regulation is done by the battery management system (also referred to as the BMS) and should take place during charging and discharging of the battery. The BMS is an essential part of a battery which monitors cell properties such as the SoC (State of Charge) and whether a cell is broken. The last part of the architecture of the battery is the thermal management section which takes heat away from the battery, which is discussed along with the BMS in Section 3.3.

3.2.1. Mission Energy Requirements

Over the course of the mission, the power requested from the battery varies and the time the power is requested for also varies. In order to ensure that the battery can handle an entire trip it will be designed with the worst case trip in mind. The worst case trip is if the cruising altitude is considered to be the ceiling altitude of the airplane which in this case is 9000 m, additionally, all auxiliary systems are constantly on during the entire mission. The rise time to this altitude is derived by the rise speed taken from the 10 passenger Citation jet [10], which is approximately 19.58 m/s. This gives a rise time of about 7 minutes 40 seconds. Furthermore, both taxiing in and out is assumed to take 10 minutes. Lastly, the competition guidelines [11] give the time for cruise and descent to be a 28 minutes (cruise duration: 12 minutes, descent duration 16 minutes). Table 3.2 shows an overview of the power requested for different parts of the mission.

Mission Part	Time (min)	Motor Power (kW)	Auxiliary Power (kW)
Taxi out	10	0	60
Ascent	7.66	1150	60
Cruise + Descent	28	515	60
Taxi in	10	0	60

Table 3.2: Mission sections duration and power requested

The value for the motor power is obtained via the competition constraints [11] and the auxiliary power is calculated in a different paper related to this project [12]. From Table 3.2 the total energy usage for a worst-case mission can be calculated. This can be done by converting the time to hours and multiplying it by the total power used in that time frame. Doing so yields a total energy of 442.81 kWh. This is, however, not taking into account the efficiencies of the electrical distribution system. For this, an estimated 92% efficiency is used for the motor to battery electrical energy and a 90% efficiency is used for the auxiliary energy. Incorporating this yields a total requested energy of 482.66 kWh.

3.2.2. Main Battery Energy Estimation

There are two limiters to the energy that the battery should store: the first is the actual energy required from the battery during a mission, the second is the power output from the battery. For higher power output, more cells have to be placed in series or parallel to increase the energy capacity of the BESS. For some cases this energy capacity is already higher than that required of the battery. In other cases the power delivered by the cells doesn't store enough energy that the battery needs to deliver. In this

case the extra cells need to be added to the architecture of the battery. With respect to this it's important to note that a battery is never used from 100% SoC to 0% SoC since cell voltage changes as a function of SoC, this change is particularly large close to the full and empty capacity as seen in Figure 3.2. This means in order to use 482.66 kWh for the mission (found in the previous Section 3.2.1) the battery must store more energy than is required for the mission. The extra amount is determined by the operating region which can be found from the charge and discharge curve in Figure 3.2. The charge curve limits the bottom boundary to about 60 mAh g^{-1} while the discharge curve limits the upper capacity boundary to about 1500 mAh g^{-1}. This means that only about 86% of the cell charge is usable as an energy supply. Therefore, 86% of the required battery energy is equal to 482.66 kWh. The total energy stored in the battery is therefore 561.23 kWh.

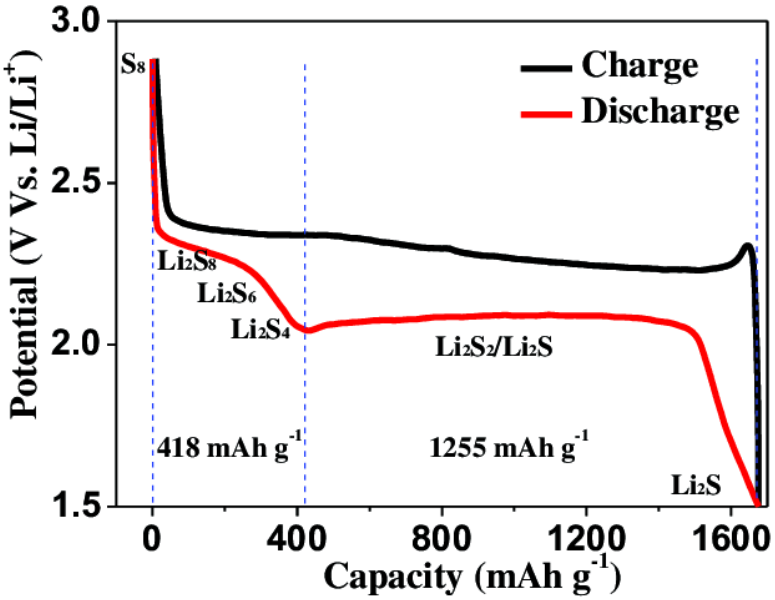

Figure 3.2: Typical charge/ discharge curve of a lithium-sulfur cell [13]

From Section 3.2.1, 715 series cells and 2 parallel cells are required for a 1.5 kV battery. This together with another 1.5 kV battery makes the bipolar, 2 MW embedded power supply that drives the aircraft. It was decided that two of these sets of batteries would be used so that there is a degree of safety if one system were to fail. The total number of cells in this system to supply the 2 MW embedded power is $715 \times 2 \times 4 = 5720$ cells. If every cell can hold approximately 42 Ah of charge then the energy each cell can hold is equal to the cell nominal voltage multiplied by the cell charge: $2.1 \times 42 = 88.2$ Wh. This means that, in order to supply the embedded power, the battery will have an energy capacity of $88.2 \times 5720 = 504.504$ kWh. This value is just shy of the minimum capacity required for a mission. This means that the batteries should carry more cells than the mentioned 5720 cells. A total number of cells can be calculated from the battery energy needs: if each cell holds 88.2 Wh of energy then $561230/88.2 = 6364$ cells are required within the battery. As long as the battery outputs the required power ($V \cdot I = 2$ MW) then it's possible to transform the output of the battery to the required voltage level. This means that different configurations of cells are possible.

3.2.3. Battery Modules and Weight Estimation

The configuration of cells and modules in a battery is quite important as it affects several aspects of the battery such as its weight and the internal resistance [14]. It's found that parallelisation in modules rather than cell strings leads to lower internal resistance as well as a lower weight. This means that if, for a battery pack, 4 parallel cells are required then it's best to put 4 modules of 1 parallel cell in parallel than 1 big module composed of 4 parallel cells. In order to optimise the number of cells in the battery, implicitly optimising the weight of the battery through minimisation of the cells, the battery should be

designed so that it has a total cell count as close as possible to 6364 cells while maintaining the ability to produce the embedded power requested. It's important to keep in mind that not too many parallel modules can be used otherwise balancing of the cells is more complex and the current given by the battery is very high, making thermal management more complicated. Keeping this in mind, this thesis will look at up to 5 parallel modules. When it comes to determining the right amount of series cell it's important to keep in mind that a larger amount of modules leads to a larger module control unit count which also means higher costs [14].

Parallel Modules	Series Modules	Series Cells per Module	Total Cells in 4 Packs
2	4	199	6368
3	9	59	6372
4	2	199	6368
5	11	29	6380

Table 3.3: Number of cells and modules for 1 out of 4 of the battery packs

From Table 3.3 it's clear that the optimum number of parallel modules are 2 or 4 since it gives a cell count closes to the required energy for a mission. It's important to note that for all of the packs shown in Table 3.3, the voltage level is different than that required of the battery. This is not a problem as a power converter can be placed directly after the battery to boost the voltage to the right amount. For both cases where 2 and 4 modules are used in parallel the total number of modules is the same. With this in mind the best choice is to go with the pack that only has 2 parallel modules since this configuration will produce less current and therefore less heat. In this case a bi-directional converter is required since the voltage level is 1671.6 V compared to the requested 1.5 kV. Bi-directional converter is required so that the battery can also charge and the duty cycle of the switches should be able to change since the output voltage of the battery changes drastically in its discharge cycle. With this in mind, and that the cells weigh about 138 g, an estimation for the weight of the cells can be made. For 6368 cells the weight would be about 878.784 kg, this weight is not including the weight of the BMS and thermal management systems. In Section 3.3 an estimate is given as the percentage of the weight of the battery that is for protection and control. The range given there is 23%-37%, the median value is 30% which will be used to calculate the total weight of the battery. Without the protection systems the battery weighs approximately 878.784 kg and with it the weight increases to 1255.406 kg. It is also found that methods already exist to decrease the weight of the entire battery by as much as 15% through optimizing the protection systems. By 2038 these methods will possibly be developed even further but for now it is assumed that the battery is 15% lighter than if conventional protection systems are used. Using these developed protection systems the battery will weigh approximately 1067.095 kg.

3.2.4. Backup Avionics Battery

In the unlikely case that both the battery systems fail, there will be a backup battery that can be switched on. This backup battery will only power control systems so that the pilot may still have some control over the plane while the engines are not powered. The backup battery will operate on the 800 V line and must supply a constant power of 20 kW. It must supply this power for 16 minutes (time of descent [11]. This means that without considering the discharge curve the battery must hold 5.33 kWh of energy. Taking the discharge curve of lithium-sulfur batteries into account from Figure 3.2, the capacity should be 6.2 kWh. Following similar steps as in Section 3.2.3, the total cells that the battery should contain is 71. The minimum number of parallel cells is 1 and therefore if the battery contains 71 series cells it will satisfy the energy requirement. The power this battery can deliver is determined by the voltage from series cells multiplied by the current the cells can deliver. This value is 50 kW therefore this cell configuration also satisfies the power needs of the system. A boost converter is required since this battery outputs approximately 149 V while 800 V is required for the system. The weight of the cells in this battery is approximately 9.8 kg which is really quite insignificant compared to the weight of the rest of the system. This weight does not account for the BMS and the thermal runaway mitigation. Following the same steps as in the previous section to determine the entire battery weight a value of 14 kg is obtained when using conventional protection systems and a value of 11.9 kg is obtained when using the more developed protection systems.

3.2.5. Battery Distribution in the Aircraft

Since the batteries weight will make up a very large portion of the propulsion system it's crucial to place it so that the center-of-mass of the plane is in the desired position. The airplane also needs to be balanced and therefore the battery packs should be symmetrically placed or along the line of symmetry. In an airplane, the lift force should act on the same position as the center-of-mass. This position is usually just behind the wing spar. This means that one battery system should be placed on the right side of the plane and one battery system should be placed on the left side of the plane to keep them close to the motors which require the most power. Lastly the avionics batteries placement is much less important because it weighs very little. For the sake of maintaining the center-of-mass, however, this battery is best placed on the line of symmetry, again just behind the wing spar.

3.3. Thermal Runaway Mitigation

To ensure safety and minimise risk of faults from the battery, the biggest problem, namely thermal runaway, has to be accounted for when working with batteries like Li-ion and Li-S. Thermal runaway is a repeating process where, most likely due to a fault or puncture in the battery, an increase in temperature happens. This increase of temperature releases even more energy and gases from the battery, which in turn increases the temperature once more. The graph below shows the temperature change and failures in the case of thermal runaway.

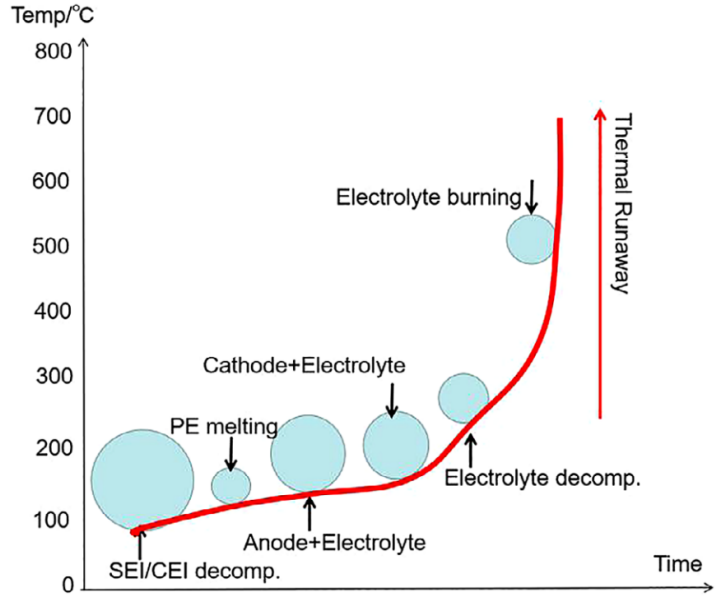

Figure 3.3: Temperature and failures over time during thermal runaway.[15]

When this process has begun it will, in most cases, have destructive outcomes for the battery and the application it is used for as seen in Figure 3.4. An example is a crashed Tesla in Switzerland, where the firemen could not control the fire using normal means due to the nature of the battery architecture [16].

Figure 3.4: Damage done to a Tesla car after the battery underwent thermal runaway. [17].

Due to the architecture of Li-ion and Li-S batteries, this issue can never fully be removed, and measures in terms of safety have to be taken to reduce risk.
Several factors can be accounted for thermal runaway in batteries such as[18]:

1. **High and low ambient temperature**:
   A high temperature reduces the ability to remove heat from the battery, causing damage.
   A low temperature raises charging time, where the battery is subject to high current for a longer time.
2. **Age of battery**:
   Old batteries need longer charging time and have higher heat generation.
3. **Internal short circuit**:
   Occurs when damage is done to the battery cells or due to bad maintenance.
   The two electrode materials touch, creating a high current density which produces heat.
4. **External short circuit**:
   Same concept as the internal short circuit, but the short circuit is formed externally instead of internally due to damage or faults.
5. **Overcharging**:
   When the battery is charged beyond the maximum capability, internal damage is done, risking higher temperatures and a shorter lifespan.
6. **Rapid charging of the battery**:
   Rapid charging uses higher than normal currents to quickly charge a battery. This high current can again lead to internal damage due to the excessive current.

As one can conclude from the list, temperature is one of the biggest problems for a battery and should be closely managed. Another consequence of a temperature increase is bulging, melting and rapturing of the casing, opening way to thermal runaway. Other issues that include damage are less common, but should get attention and sensors to detect short circuits and ensure the voltage and current caps are not exceeded.

3.3.1. Mitigation Techniques

A recent study [19] has concluded that Li-S batteries with varying electrolytes all undergo thermal runaway. This is due to the sulfur cathode and the lithium anode melting easily, creating cross-reactions which lead to thermal runaway. Therefore, mitigation techniques have to be implemented to ensure battery safety and let the user know if something is broken inside the battery. Several of these techniques, widely used in Li-ion batteries, will be discussed and used in the project.

Thermal runaway is characterised by a change in voltage and current, an increase of temperature and the release of chemical gases from the battery cells [20]. Appropriate measures should be taken combined with monitoring of these characteristics to ensure a safe operation at all times:

- Terminal voltage detection
- Overall current and voltage monitoring
- Battery deformation detection
- Internal battery temperature
- Equalised charging of the cells

Beside these electric monitoring devices, some materialistic measures should be taken as well, they include [21]:

- Heat sinks
- Cooling fans
- Heat-resistant foam
- Thermal film
- Venting
- Thermal barriers between modules
- Anti-abuse design
- Isolation of the battery system from other parts

Firstly, the Battery Management System (BMS) will be handled which will do all monitoring discussed in the first summation. Additionally, this BMS could compute some other useful values such as State of Charge (SoC), State of Health (SoH) and internal impedance of the cell.

The terminal voltage of a battery is the voltage that it provides at its terminals. This voltage should be maintained to ensure that the correct voltages are provided for the plane. If cells fail, the overall voltage of the battery lowers and is not desired. Therefore, the battery or cell modules could be turned off, and an alert can be given by the BMS.
Then, the overall current and voltages of the battery need to be monitored. The cells operate within certain voltage and current levels. If extremes in these levels occur, ie. while charging or dealing with high loads, the BMS can make decisions like lowering or nullating current altogether.

As mentioned before, battery deformation or penetration damage can harm the battery cells. This is especially prone in a plane, where many vibrations due to the motors happen and pressure changes occur that might damage the battery pack. A good and firm battery casing can help withstand these environmental variables. Sensors can be connected to the BMS that detect deformation, when the deformation is close to a threshold, the BMS warns the user and a fix can be made.
One of the most important aspects of mitigation thermal runaway is temperature control. Li-S works, as Li-ion, in a temperature interval. Especially at lower temperatures, where the chemical reactions inside the battery slow down. Studies have shown that Li-S batteries can operate at -10°C up to 55°C based on the structure of the anode, cathode and electrolyte [22][23]. Which is applicable to a plane where the temperature could lower drastically when a heating problem occurs.
The BMS will manage the battery via cooling and heating, depending on altitude, power consumption and charge state to ensure the optimal performance. For heating, a siphon can be used to recycle the heat of the battery to reduce power consumption of the heating mechanisms. Cooling of the battery can be done using air ventilation, coolants and heat sinks and overall insulation.

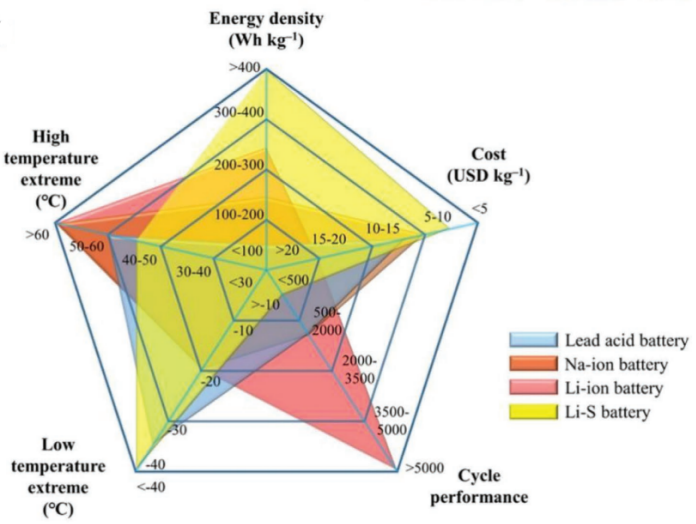

Figure 3.5: Battery type comparison on several aspects. [24]

Another important aspect that the BMS needs to manage is the equalised charging of the battery cells. When a battery discharges, not all cells discharge equally. When the battery is charged again, all cells get charged equally, this can lead to problems like overcharging if a constant charging current is provided to a fully-charged cell. Therefore, a charge equalisation circuit needs to be added to prolong the cell life and capacities. There are two main types of balancing techniques: passive and active. The figure below shows the difference between the two.

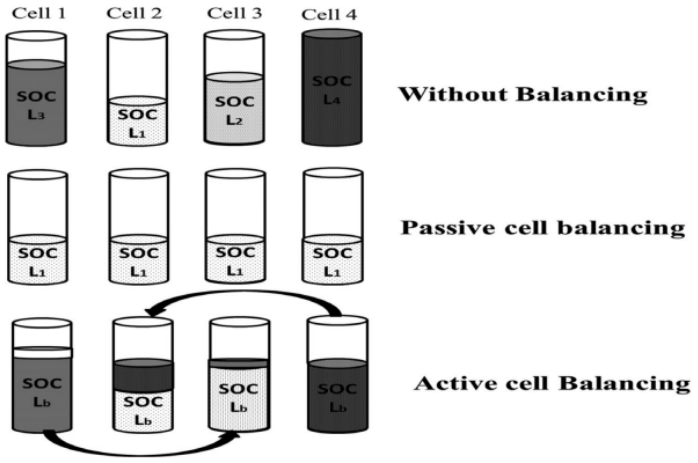

Figure 3.6: Balancing techniques based on SoC. [25]

The passive technique relies on draining the higher SoC cell while other cells keep charging. A resistor is placed parallel to the cell, and the power of the cell is drained into the resistor. A controller can monitor the cell voltages and enable or disable these resistors at the correct cells. This technique is cheap but wastes energy and brings heat to the system as the resistors heat up.

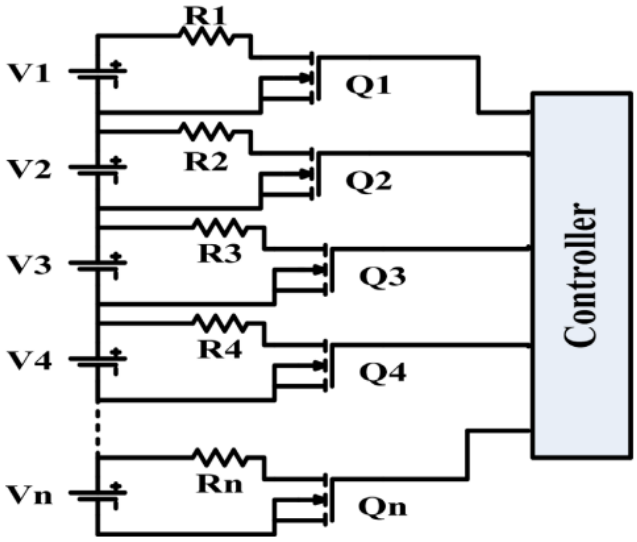

Figure 3.7: Passive balancing technique based shunt resistor. [25]

Active techniques rely on active circuit elements such as capacitors and inductors to transfer energy from a higher charged cell to a lower charged cell. They are faster and more efficient than passive circuits, but have an increased cost and complexity. Charges are stored in the capacitors or inductors and a controller makes connections between cells where needed. These circuits are good for high power applications such as our plane.
Designs using single and double capacitors or inductors have been proposed [25] where their speed and efficiency are shown to be high and that they can be used during charging and discharging. On the other hand they are shown to be expensive, very complex, in need of balancing/filters and need near-perfect switching controls.

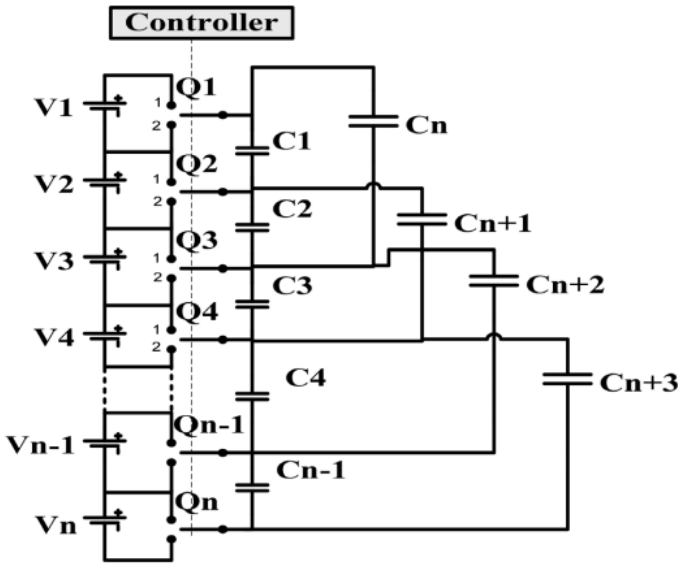

Figure 3.8: Active balancing technique using double-tiered capacitors. [25]

For our system, an active balancing circuit will be used as it is the preferred choice in high power applications.

Additional monitoring of the SoH and SoC can prolong the battery life. The SoC tells the user how

much percentage of charge is left in the battery cell. It is the ratio of current capacity ($Q_{current}$) to the nominal capacity (Q_{nom}) given by the cell manufacturer.

$$SoC = \frac{Q_{current}}{Q_{nom}} \tag{3.1}$$

Several methods are possible to estimate this value[26]:

- **Direct measurements**:
  Uses physical parameters like voltage, current and impedance to determine SoC.
- **Book-keeping estimation**:
  Uses integration of discharge current to find the SoC.
- **Adaptive systems**:
  Systems that can adjust the SoC according to the discharge situation.
- **Hybrid methods**:
  Use a combination of previously mentioned methods to determine the SoC. This has a better overall estimation.

The estimation method used in our project is the one described in [27]. Estimation techniques used in ie. Li-ion batteries cannot be used for Li-S, as the voltage curve flattens drastically at low plateau as seen in Figure 3.9. It combines a Recursive Least Squares (RLS) algorithm and Support Vector Machine (SVM), which is a machine learning method, to determine the battery states. The Li-S cell gets parameterised by an Equivalent-Circuit-Network (ECN), which models the cell as a circuit. It uses the open-circuit voltage (V_{oc}), a polarisation resistor (R_p), an ohmic resistor (R_o) and a polarisation capacitor (C_p). These parameters are put into a Forgetting Factor Recursive Least Squares (FFRLS) algorithm which will result in vector parameters for the SVM, which will estimate the SoC range. Then, the results will be combined with the Coulomb-Counting (CC) method, which estimates the SoC in real-time, to have a higher accuracy of the SoC, as the SVM only gives a specific range as value. These estimations are combined together as seen in Equation 3.2 below:

$$SoC = \frac{W_1 \cdot SoC_{SVM} + W_2 \cdot SoC_{CC}}{W_1 + W_2} \tag{3.2}$$

Where SoC_{SVM} and SoC_{CC} are the SoC estimates of the SVM and CC methods, respectively. W_1 and W_2 are fusion gains. Changing these values gives more trust in either the SVM or CC method. When $W_1 > W_2$, the SVM gets higher trust and will give a quicker convergence for the SoC. However, it fluctuates around the SoC reference. When $W_1 < W_2$, the CC gets higher trust, which gives a slower but more stable convergence to the SoC reference.
The research has shown that if the fusion gains shift from $W_1 > W_2$ to $W_1 < W_2$ during the estimation, a lower error % gets achieved. For initial values of W_1 = 0.8 and W_2 = 0.2, which change to W_1 = 0.2 and W_2 = 0.8 after convergence, a maximum error in SoC of 2.63% is found.
Lastly, tests have shown that the estimator gives acceptable results when the initial SoC conditions are less than 100%. Overall, this method is accurate, quick and not computationally-heavy, making it ideal for a fully-electric plane.

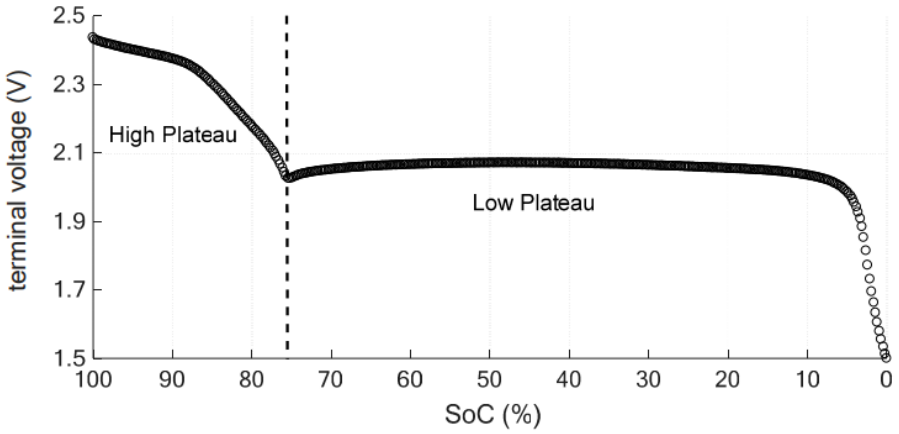

Figure 3.9: Li-S cell terminal voltage during slow discharge [28].

The SoH is the difference between a fresh battery cell and a cell in operation, which takes ageing into account. Over time, the battery's SoH will decrease from 100% due to ageing, climate, pressure, etc. An estimation technique described in [29] will be used in our design. As with the SoC estimation, parameters such as the open-circuit voltage (V_{oc}), polarisation resistor (R_p), ohmic resistor (R_o) and polarisation capacitor (C_p) will be used. The details of the technique can be found in the previously mentioned paper[29], as it is simply too much to cover in this thesis. The research shows that the estimation method has a 96.7% accuracy, which will increase over the coming years as the Li-S sector grows.

Lastly, some physical measures can be taken to improve the safety and longevity of the battery system. Many applications such as heat sinks, cooling fans, heat-resistant foam, valve venting, thermal film and thermal barriers can be used to minimise heating and heating losses, as well as keeping the battery cool during operation [21]. An anti-abuse design in the battery package greatly reduces the risk and severity of short circuits in case of deformation or a crash. Three main ways of achieving this is by using rigid, energy-absorbing structures and displacing the battery cells inside the module to lower collateral damage[21].

Additionally, it is handy to know how much the BMS and the thermal runaway mitigation precautions will weigh. To find percentages, a website [30] was consulted which listed some EV batteries used in cars. From this information, a percentage interval of 23%-37% was found. Note that these percentages are just for estimation purposes only and are not an exact value for our application, as that is beyond the scope of this thesis. Additionally, these percentages might go down in the future as better and lighter technology is developed for these applications. Then, to decrease these numbers, a recent article [31] describing a new lightweight system for thermal runaway mitigation is used. There it states that up to 15% weight of the battery pack could be shaved off.

4

Energy Transfer: Wiring System

The energy transfer system in the electric aircraft consists of cables that will carry current from the battery to the various electrical systems and instruments. When it comes to wires some important factors to consider are the voltage losses over the cable resistance, the effects and possible dangers of applying a high voltage and the temperature within the cable. Also, an estimation for the weight of the wiring system is made since weight is a large factor that affects the entire aircraft. Furthermore, something else to consider is the connection between electrical components such as between the battery and wires, wires and other wires, and between wires and circuit boards. All of the above will be discussed in this chapter.

4.1. Cable Sizing

Table 4.1 shows a brief and very approximate rundown of what the expected cable lengths are for different parts of the aircraft. A rough schematic of the aircraft can be found in Figure A.1. With the dimensions given in the schematic, the cable lengths can be estimated based on the electrical component distribution. The aforementioned table will be used in the upcoming subsections to calculate requirements and behaviour. For the sake of clarity, each wire set is given a node name for cross-referencing with figures, these nodes can also be seen in the plane schematic (Figure A.1. The low voltage wires (connected to low voltage loads) are very small and are not analysed in this thesis since they are also used in modern aircraft. For a Boeing 747 the wire length is approximately 225 km, however, this plane is approximately 5.5 times longer than the plane described in this thesis. Therefore about 40 km of small wire with diameter of 0.6 mm is assumed for this plane. This gives an approximate weight of 30.65 kg.

Voltage (V)	Power Required (kW)	Wire Length (m)	Number of Wire Sets	Node Name
3000	2000	6	1	0
3000	575	8.75	2	1
3000	575	5.8	2	2
800	30	8	1	3
800	6.1	4	2	4
800	17.5	15	2	5
800	5.5	13	2	6
800	1	8	2	7
28	1	4	1	8

Table 4.1: Approximate wire lengths within the aircraft

4.1.1. Material Consideration

There are two main materials used when it comes to conductors in wires: copper and aluminium. When it comes to selecting which one should be used in wires, one should consider the different advantages and disadvantages of both materials. When it comes to copper the main advantage is that it has a

much higher conductivity than aluminium, (copper has conductivity 58.7×10^6 S· m^{-1} while aluminium has conductivity 36.9×10^6 S· m^{-1} [32]) which means that a copper conductor will produce less heat when the same current is passed through a same sized aluminium conductor. The voltage loss over same sized cables is also smaller for copper conductors as opposed to aluminium conductors. The advantages of aluminium are that it is much cheaper than copper and it's much less dense (aluminium density: 2700 kg· m^{-1}, copper density: 8900 kg· m^{-1} [32]). One thing worth noting is that copper has a much higher melting point, however, for safety reasons, the wire should not reach temperatures high enough that aluminium would melt. The commonly used equations for the resistance per unit length of a conductor is as follows:

$$\frac{R}{l} = \frac{1}{\sigma A} \tag{4.1}$$

Where R is the conductor resistance, l is the conductor length, σ is the conductor conductivity, and A is the cross-sectional area of the conductor. From Equation 4.1 it can be seen that to get the same resistance per unit length for an aluminium conductor the cross-sectional area needs to be approximately 1.59 times larger than that of the copper conductor. Now looking at the equation for the mass of a conductor:

$$\frac{m}{l} = \rho A \tag{4.2}$$

Where m is the mass of the conductor, l is the conductor length, ρ is the material density, and A is again the cross-sectional area. Since the density of aluminium is approximately 3.3 times smaller than that of copper, Equation 4.2 shows that an aluminium conductor with the same resistance per unit length as that of a copper conductor will have approximately half the mass per unit length. This means that unless the temperature or the voltage drop is the limiting factor in one of the voltage levels for the wiring system, then aluminium is the favourable material. Regarding fire hazards, the insulation should be chosen to accommodate the temperature analysis of the conductor chosen. If the insulation stays within its operating temperature region, there is no risk of fire outside of wire failure or faults.

4.1.2. Voltage Drop

In an ideal world the entire wiring system would have a resistance of zero and therefore no voltage would drop over the conductors, however, this is never the case. All conductors resist the flow of current at room temperature and therefore there is a voltage drop over it since the charge carriers put work into moving through the conductor. The potential difference over a conductor is determined by its resistance which changes as a function of the conductor length and the conductors cross-sectional area (see Equation 4.1). What this means is that the shortest possible path should be taken for the cable and then one can consider that value fixed. These lengths can be seen in Table 4.1. Now the optimization comes from finding the cross-sectional area that corresponds to a maximum voltage drop. In the following example the case is considered where the voltage drop over a cable should not exceed 2% of the regulated voltage. Later on in this chapter different conductor sized will be analysed and the corresponding voltage drop. Consider a cable connected from the source to the load then $V_{drop} = 0.02V_{src}$ and the remaining voltage is delivered to the load: $V_{load} = 0.98V_{src}$. The current through the cable (Ohm's law) and the load ($P = V \cdot I$) can be described as:

$$I_{cable} = \frac{0.02V_{src}}{R_{cable}} = \frac{P_{load}}{0.98V_{src}} \tag{4.3}$$

$$R_{cable} = \frac{0.02P_{load}}{0.98I^2} \tag{4.4}$$

Equation 4.4 is obtained by rearranging Equation 4.3 for R_{cable} through eliminating V_{src}. Another thing to consider is that the resistance of conductors increase with temperature. This means the operating temperature should be taken into account when calculating the maximum resistance. Equation 4.5 shows how the temperature affects the resistance [33].

$$R_{cable} = R_{ref} \cdot (1 + \alpha_r(T_c - T_{ref})) \tag{4.5}$$

R_{ref} is the reference resistance, i.e. the resistance of a conductor at a given temperature T_{ref}, T_c is the actual conductor temperature, and α_r is the resistance-temperature scale factor ($\alpha_{r,cu} = 0.00394°\text{C}^{-1}$

and $\alpha_{r,al} = 00429°\text{C}^{-1}$), which defines how much the resistance increase per degree Celsius. By substituting Equation 4.4 into Equation 4.5 and rearranging for R_{ref}, one arrives at Equation 4.6. This equation describes how the maximum reference resistance of the cable must change in order to accommodate the current that will pass through it at a given temperature. Finally, rearranging Equation 4.1 for just the resistance and then substituting that into Equation 4.6 yields equation 4.7.

$$R_{ref} = \frac{0.02P_{load}}{0.98I^2(1+\alpha_r(T_c - T_{ref}))} \tag{4.6}$$

$$A = l \cdot \frac{0.98I^2(1+\alpha_r(T_c - T_{ref}))}{0.02\sigma \cdot P_{load}} \tag{4.7}$$

One thing that should be made clear is that Equation 4.7 describes the *minimum* area of a conductor to have a voltage drop of less than than 2% of the source voltage. From this equation one can see that for a wire of fixed length, uniform conductor, fixed load and maximum temperature the minimum area is proportional to the square of the current that the load demands. Increasing the supply voltage will decrease the current that passes through the wire (since $P = V \cdot I$, however, this will lead to problems which will be discussed in Chapter 5. Although this area does keep the voltage drop at less than 2%, the cable temperature is not analysed in this equation and therefore this should also be taken into account.

In order to analyse the optimal conductor size for each node, simulations were made in order to visually see how the conductor size affects different factors such as the maximum temperature reached. By approaching the problem in this way, the MATLAB code under Appendix B.1 was created. In order to illustrate the voltage drop based on the conductor size, the plot that can be seen in Figure 4.1 was created. The peak-to-peak voltage is analysed since the the two lines will both have an approximately equal voltage drop since they have the same dimensions.

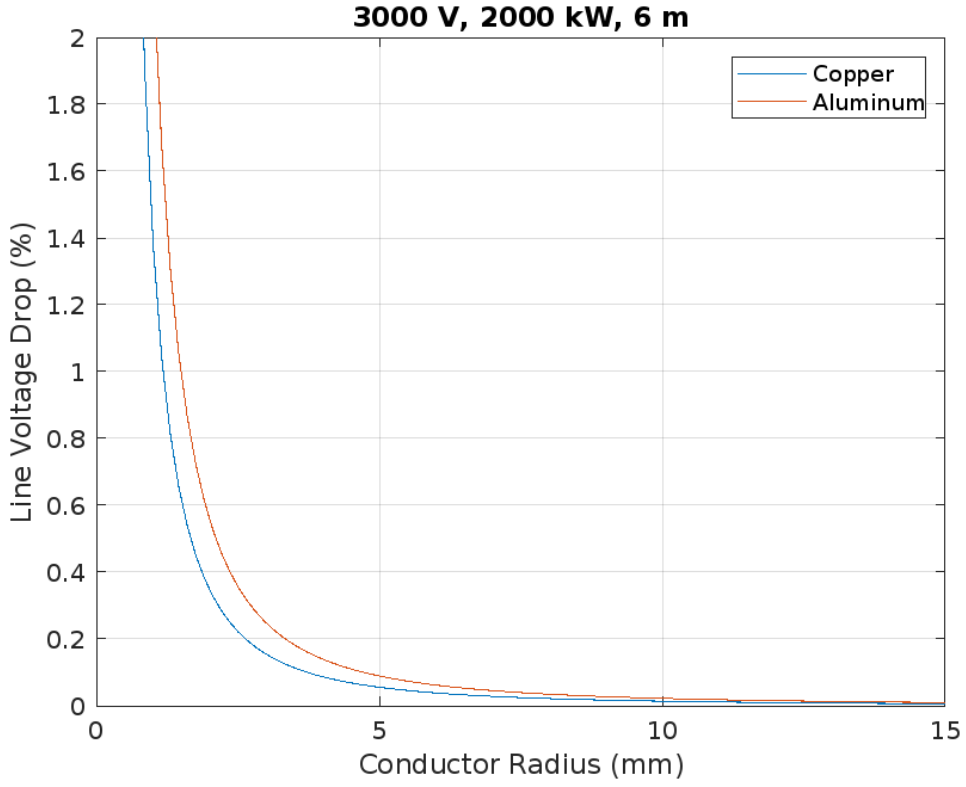

Figure 4.1: Voltage drop as a function of conductor radius for Node 0

The conductor temperature taken for this plot (T_c in Equation 4.5) is 90°C. The reason for this is that all conductors will operate at 90°C or lower and to avoid adding another variable to simulate, one can

take the worst case scenario and apply it to all the equations. In Figure 4.1 the y-axis is limited to 2% since one isn't interested in any conductors that allow a voltage drop of $>$2% of the source voltage. The voltage drop curve of the remaining 7 wires can be found in Appendix A.2 as Figures A.2 through to A.9. The aforementioned figures not only show the minimum conductor radius to keep the voltage drop at $<$2%, but also show the result of copper's higher conductivity. For the same conductor size the copper conductor has a smaller voltage loss than the aluminium conductor.

4.1.3. Temperature Analysis

When finding the right size for a conductor one also has to consider the maximum temperature reached when passing a certain current through the conductor. The chosen insulator has to be rated to withstand this temperature or else there's a risk that it will melt or catch fire. Although the insulator size is required for simulating the temperature, this report discusses the sizing of insulators in Section 5.1.2. The method for simulating the temperature will be through setting up thermal transfer equations and then simulating them over different conductor radii. The steady state temperature is reached when the heat generated is equal to the heat dissipated. In this case the heat generator is the current passing through the wire and the heat dissipation is the heat conducted away by the insulator. The heat conducted by the insulator is also a function of the heat transfer to the surroundings by the insulator, therefore the steady state heat in the conductor is a function of the heat generated in the conductor, the heat radiated from the insulator and the convection heat from the insulator. These processes are described by the following equations [34]:

$$Q_c = I^2 R_c$$
$$Q_{convection} = hA(T_i - T_{amb})$$
$$Q_{rad} = \epsilon\sigma A(T_i^4 - T_{amb}^4)$$

Where Q_c is the heat generated by the current in the conductor, I is the current in the conductor, R_c is the resistance of the conductor, $Q_{convection}$ is the heat loss due to convection, h is the convection thermal coefficient, A is the outer area exposed, T_i is the insulator temperature, T_{amb} is the ambient temperature, Q_{rad} is the heat loss due to radiation, ϵ is the emissivity of the insulator, σ is the *Stefan-Boltzmann* constant. Since R_c is again dependant on temperature, the worst case is taken to eliminate an extra variable influence. This worst case is the resistance at the temperature of 90°C given by Equation 4.5. The value of h used in this simulation will be 11 $W \cdot m^{-2} \cdot C^{-1}$ based on the range given in [34]. Furthermore, the value of σ will be taken as 5.67×10^{-8} W$\cdot$ m$^{-2}\cdot$ C^{-4} [34]. The insulator is assumed to be a grey body and therefore an emissivity of 0.8 is assumed. To find the steady state temperature the heat input has to be set equal to the heat output as follows:

$$Q_c = Q_{convection} + Q_{rad} \tag{4.8}$$

Usually the radiation heat transfer term Q_{rad} is negligible compared to the convection heat transfer term. To test this assume one can assume a insulator temperature of 90°C (this will be the highest temperature of the conductor so this is an overestimate of the radiation transfer). Using this the $Q_{convection}$ term equates to 660 W/m^2 while the Q_{rad} term equates to 3.27$\times 10^{-4}$ W/m^2. The difference is extremely large and therefore this term can indeed be ignored. Substituting the respective equation for each heat transfer term into Equation 4.8, an equation forms which can be solved for the steady state temperature of the insulator. This equation can be seen in Equation 4.9.

$$hAT_i = I^2 R_c + hAT_{amb} \tag{4.9}$$

Together with Equation 4.5 a system of simultaneous equations is formed which can easily be solved in MATLAB (code can be found under Appendix B.1). This steady state temperature is that of the surface temperature at the insulator while the actual temperature that the insulator has to withstand is that generated by the conductor. To find this more equations are necessary. Equation 4.10 and 4.11 show how to obtain the conductor temperature [35].

$$T = \frac{1}{2\pi k} \ln\left(1 + \frac{t_i + t_{sc}}{r_c}\right) \tag{4.10}$$
$$\Delta\theta = T_c - T_i = T \cdot W_{loss} \tag{4.11}$$

Where T is the thermal resistance, k is thermal conductivity of the insulator (has value of 0.28 $WK^{-1}m^{-1}$ for cross-linked polyethylene), t_i is the insulator thickness, t_sc is the semiconducting layer thickness, r_c is the conductor radius. This is used in $\Delta\theta$ which is the temperature difference between the conductor and the insulator surface, and W_{loss} is the heat generated per meter in the conductor. The steady state temperature as a function of conductor radius can be seen in Figure 4.2. The temperature profiles for the other wires can be found under Appendix A.3 from Figures A.10 through to A.17.

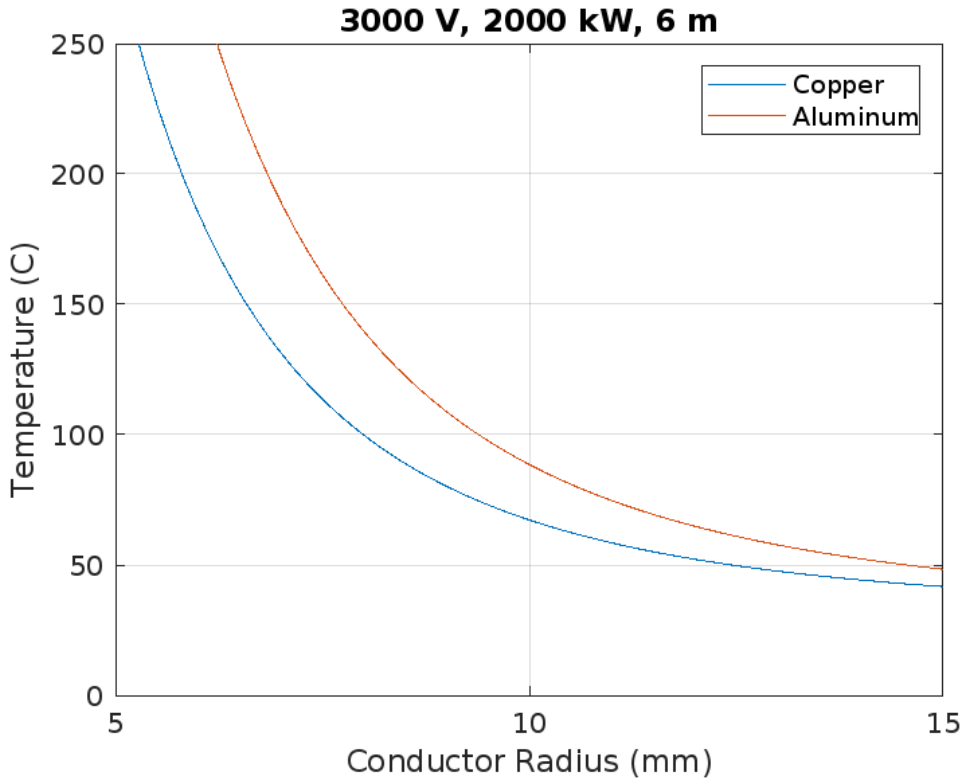

Figure 4.2: Steady state temperature as a function of conductor radius for Node 0

Figure 4.2 shows that copper has a lower steady state temperature for the same conductor size as an aluminium conductor. This is because of coppers higher conductivity. The trade-off for this is that to get a nice steady state temperature for a copper conductor, the mass will be much larger. From Figure 4.2 one can see that if you choose a copper conductor with radius 6mm then the insulator has to be rated for 90°C. If an insulator is required with a lower rated temperature then the designer must choose a larger conductor radius or a different conductor material.

4.1.4. Weight Estimation

When estimating the weight, all dimensions of the cable should be known as well as the individual dimensions of all the layers of the cable such as the insulator thickness and the semiconducting layer thickness. This is, however, not discussed in this chapter. These thicknesses and the method behind their calculation can be found in Chapter 5. The simulations that will be presented in this section will include the weights of all the layers in the cable since the MATLAB script can fetch these values easily. It's worth noting that the shield and the conductor together make up about 97% of the cables mass for copper conductor and 95% for aluminium conductors. The method for estimating the mass of the cable is done by using the density of the materials within the cables. For this calculation the density of the semiconducting layer is assumed to be the same as the density of the insulating layer. The equation for mass as a function of density and volume can be seen from Equation 4.2. From this the dimensions of the cylindrical conducting layer and other hollow cylindrical layers can be inserted into the equation. Multiplying both sides by the respective length of the cable gives the mass of the individual cables.

$$m_c = \rho_c \cdot \pi r_c^2 \tag{4.12}$$

$$m_{sc} = \rho_i \cdot \pi((t_{sc} + r_c)^2 - r_c^2) \cdot l \tag{4.13}$$

$$m_i = \rho_i \cdot \pi((t_i + t_{sc} + r_c)^2 - (t_{sc} + r_c)^2) \cdot l \tag{4.14}$$

$$m_s = \rho_s \cdot \pi((t_s + t_i + t_{sc} + r_c)^2 - (t_i + t_{sc} + r_c)^2) \cdot l \tag{4.15}$$

The equations above describe the mass of each layer, Equation 4.12 the conductor mass, 4.13 the semi-conducting layer mass, 4.14 the insulating layer mass, 4.15 the shield layer mass. The total cable mass is the sum of the mass of all the layers. The mass of the plastic jacket layer is not considered here since its mass is negligible. The equations above were simulated in MATLAB to give the masses of cables as a function of the conductor radius.

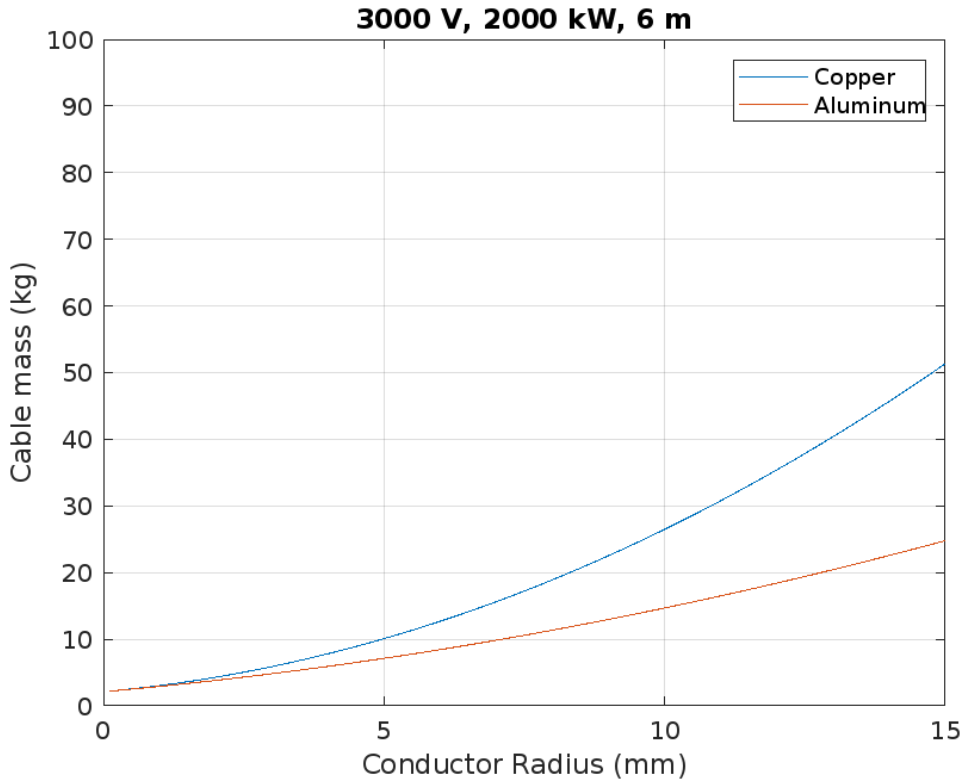

Figure 4.3: Cable mass as a function of conductor radius for Node 0

Since the mass is a linear function of cross-sectional area and cross-sectional area is a quadratic function of radius, that means that the mass of the cable is also a quadratic function of its radius. This is reflected in Figure 4.3. The cable mass quickly increases with larger conductor size. This is where the optimisation with the temperature and voltage drop comes from. While a larger conductor size does make the wires less susceptible to combustion and melting, it also significantly increases the weight of the cable system which is not desired on an aircraft. This is also where it can be seen that aluminium might be a more desirable material as a conductor because of the sheer difference in cable mass. The cable masses for the rest of the nodes can be found under Appendix A.4 in Figures A.18 through to A.25.

4.1.5. Wiring Results

By using the methods mentioned above one can select the kind of cable conductor that will be used as well as an estimate of the cable system weight. In order to choose the right conductor size one should balance the steady state temperature with the voltage drop and the weight. An overview of the choices made for each node can be seen below in Table 4.2. All conductors are made out of aluminium because of the significant weight difference.

Node	Cond. Radius (mm)	Voltage Drop (V)	Temp. (°C)	Weight (kg)	# of Wires
0	10	0.69	90	14.75	3
1	4	1.74	90	8.68	6
2	4	1.16	90	5.75	6
3	1.1	4.64	90	4	3
4	0.6	1.44	40	1.72	6
5	0.86	7.4	66	6.95	6
6	0.52	5.6	41	5.43	6
7	0.3	1.84	31	3.11	6
8	2.1	0.54	41	2.6	3

Table 4.2: Cable properties for the different nodes

All the weights in Table 4.2 need to be multiplied by three since the aircraft has 2 lines for a positive and negative (bipolar) voltage and one ground wire. Some of the nodes have 2 sets of wires which can be seen in Table 4.1, this is because the wires need to run on the left and the right side of the plane to retain symmetry. The total number of wires for each node can be seen on the right side of Table 4.2. Taking the above mentioned into account, the total weight of the wiring system (including the small wires) in this aircraft is approximately 284.54 kg. There is a large margin of error in this number since the wire lengths are very rough estimates. In order to reduce the weight of the cable system, insulation should be used that can withstand higher temperatures, however, this will also increase the voltage drop over the wire.

4.2. Connectors

When dealing with electrical distribution systems one also has to consider how the different systems are interconnected. There are three main connection in the aircraft wiring system: battery-to-cable connection, cable-to-cable connection, and cable-to-board connection. It's possible to use different types of connectors for each of the above mentioned connection, which provide different advantages and disadvantages.

Battery-to-cable connection

When it comes to the battery-to-cable connection the chosen connector was lugs. Lugs provide a contact for electrical transfer by screwing a piece of metal connected to a cable onto the battery contact. There is a hole for where the lug will be screwed onto the contact of the battery. It is also possible to insulate lugs so that the high voltage will not cause partial discharges. They are usually used when an electrical wire needs to be removed from what its connected to quite often. A large problem when it comes to high voltage is wear and tear in cable due to partial discharge. While steps have been taken to prevent partial discharges from occurring in the insulation, the insulation will always weather down while in use. By using lugs the cables can easily be replaced or removed for inspection.

Cable-to-cable connection

Two types of connectors were considered for cable-to-cable connections: a terminal block and junction box. Throughout the aircraft there are T-junctions of cables which means that one cable splits off into two separate cables. In order to do this safely a connector is required with some considerations. The box has to have been tested so that if a high-voltage is applied to the cables within the box, there shouldn't be partial discharges between the cables. This is done in the development stage of the junction box/terminal block. The advantages of the junction box are that the wires within the junction box have a lot of protection from any damage while its disadvantage is that it has relatively high maintenance costs. The terminal blocks advantage is that it is smaller, however, through the vibrations of the aircraft it's possible that the terminal block could nick a wire, which could lead to dangerous situations. Considering the damage could be detrimental, the junction box is the better option. Furthermore, the junction box can be filled with an insulating material to help mitigate partial discharges.

Cable-to-board connection

The final connection type is the cable-to-board connection. For this connection the terminal block is used. The most important consideration for implementing this connector is reducing the vibration where the connection is made in order to reduce the risk of nicking the wire. This can be done through using dampers on the circuit board and on the wire close to the connecting point. The terminal block allows the input wires to split off into the required signals that the circuit board requires. Another thing to consider is that, for higher voltage levels, the wires are quite thick. This should be taken into account when selecting the terminal block.

5

High-Voltage Considerations

The uniqueness of the aircraft is that it is fully electric in that it does not use any combustible fuel to provide propulsion. Therefore all of the vast power required to propel the aircraft is provided by an electrical system. In order to keep the current at a controllable level, high voltage is required, which comes with its own challenges and considerations. When dealing with high voltage a variety of hazardous events can occur which need to be considered when developing a suitable electrical distribution system. These hazardous events become even riskier when dealing with low-pressure situations. At lower pressures the breakdown voltage of air decreases making it easier for arcs to jump between surfaces and for partial discharges to occur. This is what this chapter will discuss and how to reduce the chance that these faults happens.

5.1. Partial Discharge Mitigation

Partial discharge is a phenomenon in which a strong electric field causes a partial breakdown in a dielectric which in turn causes a discharge through the dielectric [36]. This partial discharge usually takes place in an air gap. These air gaps (also called voids) are unavoidable faults in the insulation that occur in the manufacturing process. This phenomenon is most common in high voltage cases because this is where the electric field is strong enough to cause a partial discharge. In the case of an electric aircraft, the voltage level is already considered high at voltage levels above 300-550 V. The reason for this is that at higher altitudes the air pressure decreases and thereby the breakdown voltage of air also decreases. This decrease in breakdown voltage allow high-voltage phenomenon such as partial discharge to occur much easier.

5.1.1. Breakdown Voltage At High Altitudes

The ceiling altitude at which the aircraft cruises is at 9 km above sea level which means that this should be taken as the worst case scenario in which the electrical distribution system should still function. The 9 km worst case altitude also presents the lowest pressure that the flight will experience. Figure 5.1 shows how the atmospheric pressure changes as a function of the altitude using sea level as a reference. At an altitude of 9 km the corresponding atmospheric pressure is approximately 32.5 kPa. This pressure can be used to find the breakdown voltage as a function of void size.

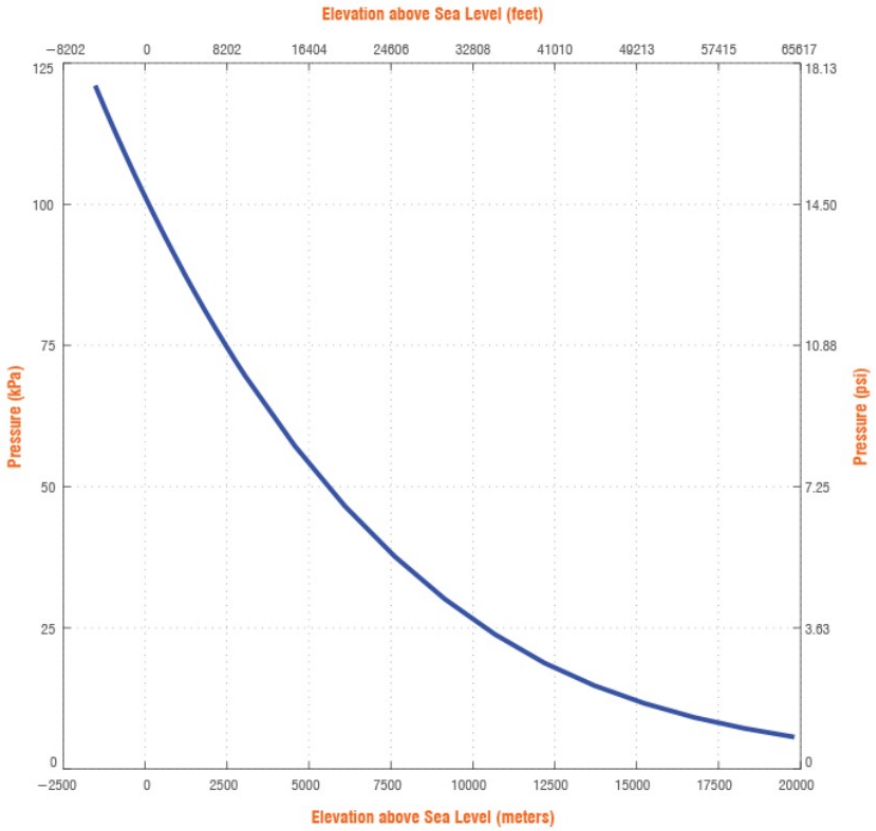

Figure 5.1: Atmospheric pressure as a function of altitude [37]

Paschen's curve is used to find the breakdown voltage as a function of the product between pressure and distance. The units for the pressure distance product given in Figure 5.2 is bar·mm, therefore to use this Paschen curve the pressure should first be converted from kPa to bar. 32.5 kPa is equivalent to 0.325 bar. A manufacturing standard for insulators is that a void size should not be larger than 50 μm. On the Paschen curve in Figure 5.2 this gives a breakdown voltage of about 250 V.

A breakdown voltage of 250 V means that if the produced void gap between the electric field strength and the distance of the cavity is greater than 250 V then a partial discharge will occur. There are three main methods to reduce the frequency of partial discharges in insulation, namely: increasing the insulation thickness, changing the insulation material or making sure that all voids are small enough that partial discharges will not occur. Partial discharges can also occur on the surface of the insulator. To battle this a metallic shield can be used since it prevents the electric field from traversing any further.

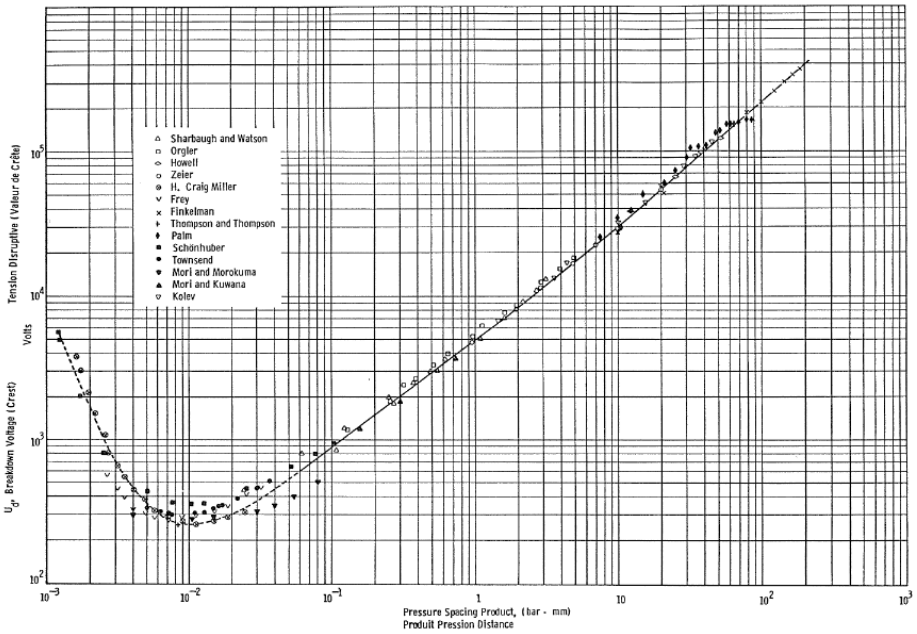

Figure 5.2: Paschen's curve [38]

5.1.2. Insulator Sizing

The method used for calculating the thickness of insulation is known as the SVD method described in [39]. The method is not dependent on the conductor material which allows for an analysis of copper and aluminium conductors in one equation. The insulation thickness is highly dependent on the maximum voltage that is applied over the cable since a higher voltage also produces a much stronger electrical field and therefore thicker insulation is required. There are different forms of voids within insulation namely [40]:

- **A**: Spherical cavities
- **B**: Fissures between the electrode and dielectric
- **C**: Fissures in the direction of the electric field

The electric field in cases A and B is stronger than the electric field in the dielectric by a factor of K given by:

$$K = \frac{3\epsilon}{1 + 2\epsilon} \tag{5.1}$$

This means that partial discharges are more common in the case of A and B. However, the partial discharges are more dangerous in the case of C as it bridges a larger part of the dielectric [40]. The factor given in Equation 5.1 is also used in the equation to calculate the insulation thickness. The equation to calculate insulation thickness is given by [39]:

$$T_i = r_c(\exp\left[\frac{K \cdot V_{max} \cdot t_v}{\alpha \cdot r_c}\right] - 1) \tag{5.2}$$

Where T_i is the thickness of the insulation, r_c is the conductor radius, K is the form factor of the void given in Equation 5.1, V_{max} is the maximum voltage that will be applied to the conductor, t_v is the maximum void size, α is the breakdown voltage given in the previous subsection. Another proposition is the use of a constant in order to match low-voltage cables and empirical formulas[33]. Equation 5.2 then becomes:

$$T_i = r_c(\exp\left[\frac{K \cdot V_{max} \cdot t_v}{\alpha \cdot r_c}\right] - 1) + C \tag{5.3}$$

Where C takes the value of 0 cm when the maximum voltage is greater than 20 kV and 0.1 cm for any maximum voltage under 20 kV. This way even if a very low voltage is used, the equation will still

give an insulation of at least 1 mm. Through looking at currently available aviation ready cables, the most commonly used insulation material is cross-linked polyethylene (XLPE) rated at 90°C [41]. This insulation is suitable for all cables given in Table 4.2. Some properties of cross-linked polyethylene: dielectric permittivity (ϵ) of 2.3, material density (ρ) of 930 kg/m^3. Using the aforementioned values for the dielectric constant in Equation 5.1 and by extension Equation 5.3 the insulation thickness can be found as a function of conductor radius. This curve can be seen in Figure 5.3. The insulation thickness curves for the other nodes can be found under Appendix A.5 in Figures A.26 and A.27. Because Equation 5.3 does not depend on the cable length or the current flowing through the cable, only 3 insulation thicknesses are necessary. Although the title of the figure shows 3000 V, this is simply a label for the voltage level the wire is designed for. The simulations were carried out at the bipolar voltage levels (1500 V, 400 V, 12 V).

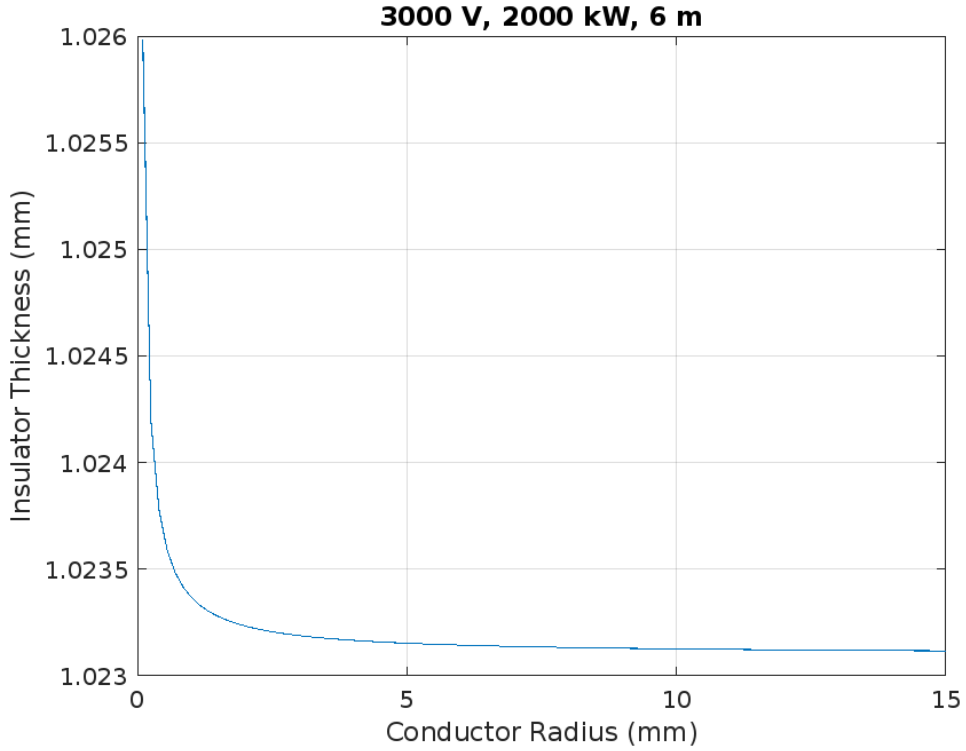

Figure 5.3: Insulation thickness for nodes 0 through to 2

The conductor radius can be read off of Table 4.2 to find the insulation thickness which should be rounded upward to ensure that the thickness is large enough to contribute to reducing the risk of partial discharges. Although a larger thickness helps against partial discharges, making the insulation larger and larger has diminishing returns in terms of preventing partial discharges.

The much more effective way of preventing partial discharges is making sure that the manufacturer does not create cavities larger than the threshold provided. To do this one must consider the worst case scenario electric field in a void: when the void is a horizontal fissure. The electric field in this type of void is equal to ϵ_rE, for cross-linked polyethylene the electric field is 2.3 times stronger in the cavity. What's more, since the conductor size is much larger than the insulation thickness, one can assume that the electric field within the insulator is uniform and can be described by E=V/d. For the highest voltage wire, this electric field can be calculated using the values found later in Table 5.1. The strongest part of the electric field is the electric field closest to the conductor which will have a value of $\frac{1.5kV}{1.1mm}$ = 1.36 kV/mm. This means if there is a void very close to the conductor, the electric field within this cavity will be 2.3 times larger: 3.14 kV/mm. The product of the electric field and the void size should be less than the breakdown voltage found on the Paschen curve using the same void size. The maximum void size is the value of the void size that gives the same breakdown voltage from multiplying 3.14 kV/mm by the void size as using the Paschen curve. From inspection, this value is around 210

μm. The voltage due to the electric field is, in this case, approximately 660 V. The pressure-distance product is approximately 6.8×10^{-2} which gives an equivalent breakdown voltage of approximately 660 V. This means that if the size of the void exceeds 210 μm, a partial discharge will occur.

5.1.3. Semiconducting Layer

There are two main reasons that high voltage cables use semiconducting layers in their architecture: uniforming the electric field and to avoid new cavities forming due to thermal expansion and compression [42]. It is impossible to produce a perfectly smooth conductor because there will always be slight imperfections on the surface. Sharp edges cause the strength of the electric field to increase drastically. Figure 5.4 shows this effect. In Figure 5.4a, the voltage produces electric fields of magnitude 16 kV/mm while in Figure 5.4b the electric field close to the conducting layer is 12 kV/mm. A weaker electric field means the voltage across the voids will also be lower.

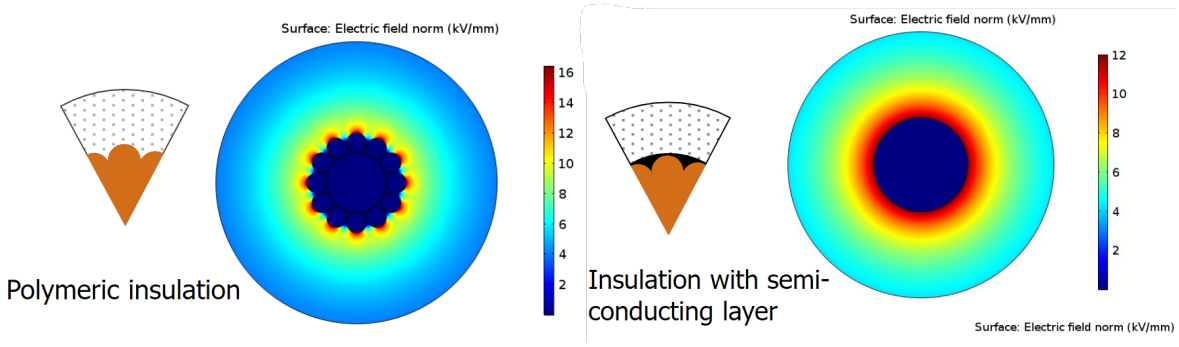

(a) Electric field with only an insulating layer

(b) Electric field with a semiconducting layer

Figure 5.4: Electric field in the absence and with a semiconducting layer [43]

While the cable is active it heats up due to the current passing through it. When materials heat up they expand and when they cool down they compress back down to their original size. This expansion and contraction can cause cavities to form in between the electrode and the insulation where partial discharges can occur. The semiconducting layer that is placed in between the conducting layer and the insulation layer closely connects the two so that the formation of these air gaps is less likely [42]. The thickness of the semiconducting layer varies from cable to cable. In this implementation a semiconducting thickness of about 1.2 mm will be used [44]. While aviation cables and underground cables have different environmental requirements, both types of cables need to prevent internal and surface partial discharges.

5.1.4. Shield Layer

Coating the insulator is the metallic shield. There are three main reasons why a shield is used in a cable with the most important one being that it helps against partial discharges between two cables. The way it does this is that by encapsulating the electric field in a hollow conductor it causes the field outside to be zero. Where there is no electric field, a discharge cannot occur. The other two reasons for the shield is that it helps prevent cross-talk between data which can impede the signal on either line. Lastly, shielding protects data lines from electromagnetic radiation which can cause a larger noise signal which reduces the signal to noise ratio within data lines. It's important to note that the shield is a grounded conductor since the short circuit current should flow to ground. Following from this, the thickness of the shield is determined through the short circuit current that will flow through due to a full breakdown of the insulator. When a full discharge occurs, the current flows through the insulation and into the shield. The heat generated by a short circuit current is dependant on the thickness of the shield since a larger cross-sectional area means lower resistance so less heat power. Commercially available cables use shields with thickness ranging from 1 mm to 2 mm [41]. The cables stated are for voltage levels around 600 V, therefore a thickness of 2 mm is more suitable for the cables used in this project. A very basic analysis can be done of the temperature change of the shield when a short circuit current is passing through by using Joule's law of heating. The law is summarised by the equation:

$$Q = I^2Rt \tag{5.4}$$

Where Q is the heat energy, I is the current passing through a conductor, R is the resistance of the conductor, and t is the time the current is applied to the conductor for. Using Equation 5.4 in combination with the equation of specific heat:

$$Q = mC\Delta T \tag{5.5}$$

Where Q is again the heat energy, m is the mass of the heating element, C is the specific heat capacity of the heating element, and ΔT is the temperature change. The temperature change can be found by equating Equations 5.4 and 5.5 and rearranging for ΔT as follows:

$$\Delta T = t\frac{I^2R}{mC} \tag{5.6}$$

The largest short circuit current will come from a full discharge that occurs very close to the battery. Therefore the short circuit current can be found as the battery voltage divided by the internal resistance of the battery. Using the above equations a temperature increase can be found as a function of the conductor radius (the insulation thickness is found as a function of the conductor radius). This can be seen in Figure 5.5.

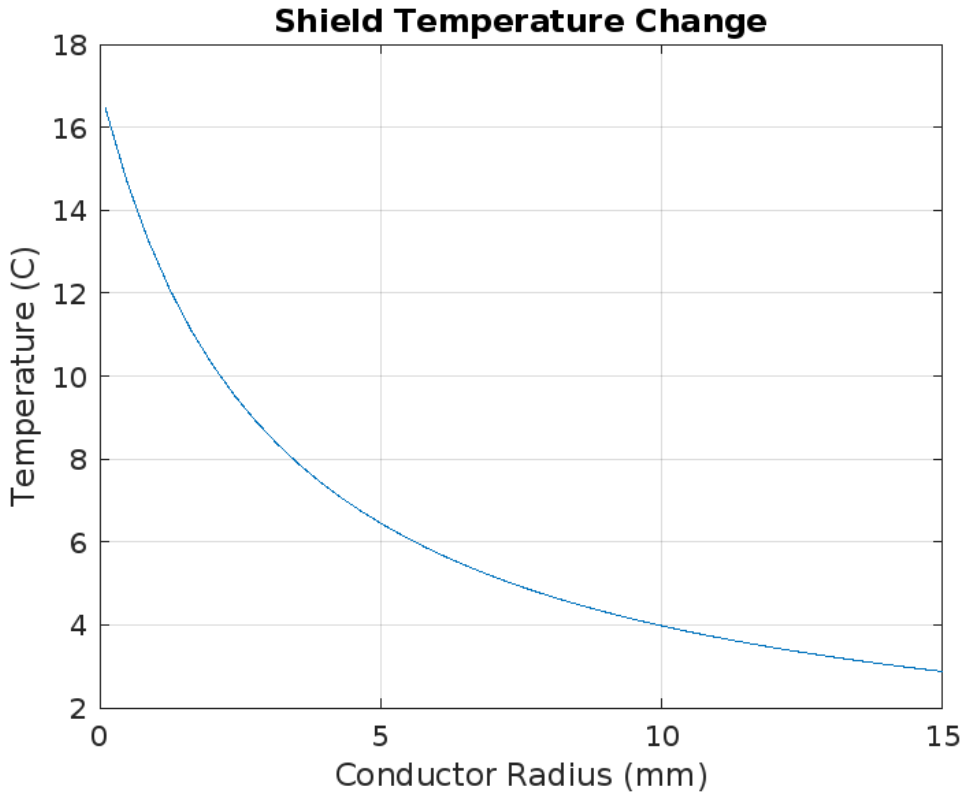

Figure 5.5: Temperature change in the shield of the cable

For the simulation seen in Figure 5.5, a short circuit duration of 300 μs is used which is an estimation for the time it takes for the breaker to react to the fault [45]. Furthermore, copper is used as the shield material since the temperature of the shield needs to stay low while the mass of the shield also helps to lower the temperature generated from a short circuit current according to Equation 5.6. Finally, an internal resistance of 50 mΩ is assumed. The simulation shows that the temperature does not exceed the cable conductor temperature cap of 90 degrees. This means that this shield thickness is acceptable for the wiring system.

5.1.5. Cable Dimension Summary

In this section the insulation thickness was found based on the breakdown voltage and as a function of the conductor radius. The semiconducting layer thickness and the shield layer thickness were also found. The last layer that fits over the entire cable is a plastic jacket which insulates the shield as well as mechanically protects the wire. The semiconducting layer thickness was assumed to be about 1.2 mm and the metallic shield thickness was assumed to be about 2 mm. From Table 4.2 and Figures 5.3, A.26, A.27 the insulation thickness can be found. The insulation thicknesses (rounded upward) and total cable diameter can be found in Table 5.1.

Node	Cond. Radius (mm)	Insulation Thickness (mm)	Cable Diameter (mm)
0	10	1.1	28.46
1	4	1.1	16.46
2	4	1.1	16.46
3	1.1	1.1	10.62
4	0.6	1.1	9.62
5	0.86	1.1	10.14
6	0.52	1.1	9.46
7	0.3	1.1	9.02
8	2.1	1.1	12.62

Table 5.1: Insulation thicknesses and total cable diameter for each node

5.2. Parallel & Series Arc Mitigation

Another big safety hazard when it comes to wiring are electric arcs. These are discharges of electricity that carry immense heat and can expel molten particles of wiring into the air, causing fires and meltdowns. There are two main arcing faults: series arcing and parallel arcing.
Series arcing occurs when a cable has a deformation/break and the current cannot pass through as normal.
Parallel arcing occurs between two cables, where a cut in the wiring of both cables enables an arc between the two. This type of fault can be seen as a short-circuit or a ground fault, where the parallel arc is between the cable and ground.
The figures below show the difference between these arcs.

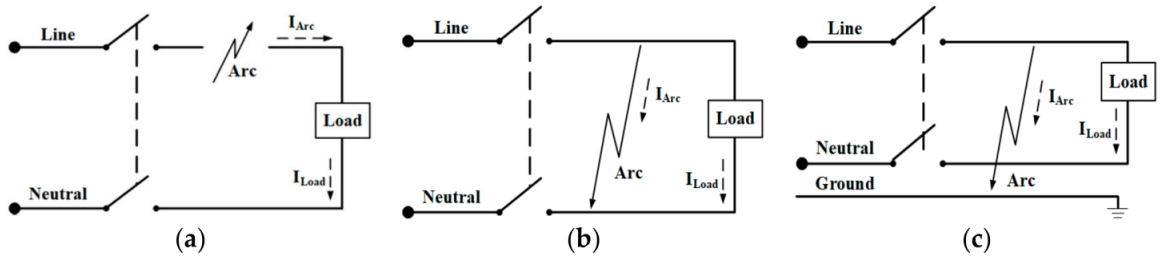

Figure 5.6: Arc fault types: a) series arc, b) parallel arc, c) ground arc. [46]

Figure 5.7: Arc faults as seen on wire level. [47]

As mentioned before, these arcs have a fire hazard, which can be disastrous in an airplane. Because the voltages and currents used are high, extra caution and safety equipment regarding arcing have to be kept in mind. In planes, these faults in the cables can occur due to several reasons such as:

- Vibrations causing chafing, which loosens the wiring from the sheath.
- Overall cable stress due to temperature and pressure differences.
- Moisture damage due to changing climate.
- Damage done by tools during maintenance.

In the following sections, techniques to detect and mitigate these kinds of failures will be discussed.

5.2.1. Series Arcing

The first arcing fault that will be discussed is the series arc. On average, it is more difficult to detect these kinds of arcs, as they are characterised by a lowering of current. This is, opposed to parallel arcing where the current increases, harder to determine, as currents can lower drastically during operation, ie. comparing take-off currents and cruising currents. Luckily, the damage done by a series arc is relative, as it cannot exceed the load current. A current comparison between series and parallel arcs can be seen below.

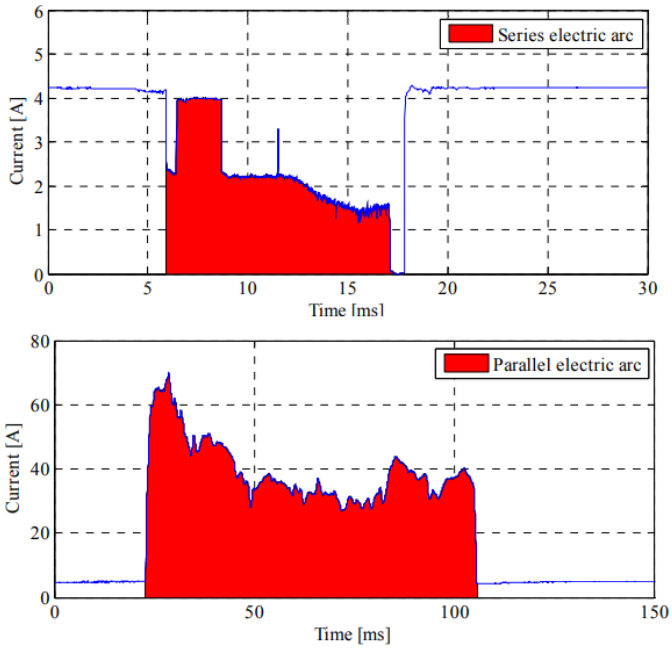

Figure 5.8: Current characteristics of arc faults. [48]

A paper from 2013 [48] describes a method to detect series arc faults in DC aircraft power networks, ideal for this application. To distinguish the series arc waveform from a normal operating waveform, three characteristics are monitored to check for series arcing:

1. A fast and steep decrease of current.
2. Current variation during arcing is much higher than during normal operation.
3. The duration of the arc.

Firstly, the current signal is monitored. To measure the rate of change of the current, its derivative is taken. The current signal is affected by noise and disturbances, which in turn get amplified in this differentiation process. Therefore, the current signal gets sent through a high-pass filter, ensuring that slow variations are discarded. The cut-off frequency of this filter is set to 1 kHz, which is based on the MIL-STD-461E standard, which states that the current must feature negligible energy above 1 kHz.
Secondly, the duration of the arc is estimated. The method utilises the variance of the filtered current.

$$\sigma^2 = var[i(t-T)] \tag{5.7}$$

Where i is the filtered current and T is the time window. When a series arc starts, the variance rises as the arcing produces high spectral components in the filtered signal. When the arc finishes, the fluctuations in the current signal quickly decrease, which in turn decreases the variance of the signal again. The total arc time can then be measured from the beginning of the arc to the moment it returns to the average current value before the arc happened. This is simply done by checking the mean value of the signal.

$$i_{average} = mean[i(t-T)] \tag{5.8}$$

The study found that the arc ending most commonly occurs when the variance σ^2 is below 110% of its original value and when the average current $i_{average}$ is above 90% of its original value.
Thirdly, the dissipated energy during the arc is computed. When a series arc occurs, the voltage drops which can be modeled by a series resistor R_{arc}. Supposing that the load resistance R_L and the supply voltage V don't change during the arc, it can be concluded that the value of the arc resistance is as follows:

$$R_{equivalent} = \frac{V}{I} = R_L + R_{arc} \quad \text{[during arcing]} \tag{5.9}$$

$$R_{arc} = R_{equivalent} - R_L \tag{5.10}$$

Then, to compute the dissipated energy, the integral of the power with respect to time is taken:

$$P = V \cdot I = R \cdot I^2 \tag{5.11}$$

$$W_{arc}(t) = \int_0^t R_{arc}(t) i^2(t) dt \tag{5.12}$$

Unfortunately, this W_{arc} is not useful, as mechanical switching could produce some arcing while in a safe operation mode. The occurrence of these grows the W_{arc} indefinitely, making it ineffective to detect an arc. Therefore, the study proposes a solution for this problem. By low-pass filtering the power dissipation, the switching frequency can be taken into account. Now, when a series arc occurs, the W_c increases, and the arc can be detected when it crosses a certain set threshold.

$$W_c(s) = \frac{P_{arc}(s)}{\omega_c + s} \tag{5.13}$$

This method of series arc detection has undergone several tests that validate the capability of the algorithm. Therefore, this detection method will be used in this project.

5.2.2. Parallel Arc

The parallel arc is characterised by a quick and high increase of measured current. Therefore, it is the most dangerous of the two arcing phenomena, as it exponentially increases the thermal energy that can result in fires.
This type of arc can be divided into two variations: a parallel fault a ground fault. The difference is simply that the ground fault is between a line and the ground, whereas the parallel fault is between lines.
Fortunately, these faults can be mitigated by standard overcurrent protections, which brings us to the next section.

5.2.3. Protection Components

To actually mitigate the arc, circuit elements called Combination Arc Fault Circuit Interrupters (CAFCI) are used. These are the upgraded version of the older Arc Fault Circuit Interrupters (AFCI). CAFCI devices protect against both series and parallel arcing, whereas AFCI devices only protect against parallel arcing. These devices detect the anomalies in the current, and it terminates the electricity flow to protect against further damage. A study, going as far back as 1999 concluded that AFCI devices were already superior to military-grade circuit-breakers, and could be used on airplanes[49]. These CAFCI devices are commonly used in households and can be extended for higher power applications like our plane.

Another type of component that can be used are differential relays. These measure the difference between sent and received current, and can terminate the transmission if that difference exceeds a certain threshold[50].

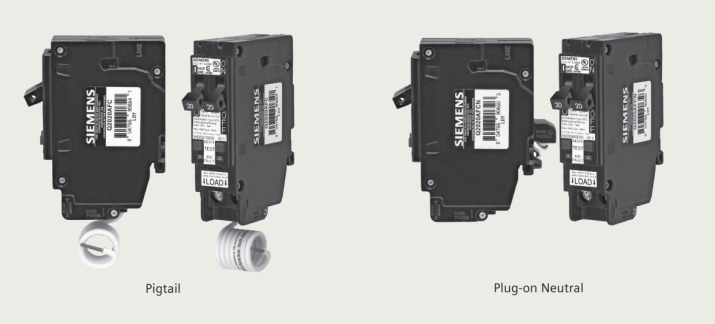

Figure 5.9: CAFCI examples. [51]

6

Reflection and Discussion

6.1. Intergroup Results

Before discussing and reflecting on our own work, a discussion about the other subgroups is held, what they achieved and more importantly, the weight of their respective tasks.

The *Power Converter and Safety* group has successfully implemented and designed the power converters, their topology, the switching frequencies of both voltage and current as well as estimated a weight for the converters used in the design. This weight comes to around 417 kg total weight of converters. Then, safety considerations have been discussed, more in-depth than in this thesis, such as mitigating critical faults, how redundancies are provided, how protection components work and their respective risks, as well as the overall electric distribution in the plane.

The *Electric Motor and Power Distribution* group has successfully discussed the electrical motors, their technology, the relevant characteristics and their mass, efficiency and size to ensure a working flight. Information regarding the power distribution, location of all components together with an optimisation of the current and voltage have been derived and given.
They give a motor weight of 153.7 kg which is including the power electronics, which comes down to 128.9 kg per motor if those are neglected. The total weight of the motors accumulates to 515.6 kg.

Overall the propulsion system described in the program of requirements in Chapter 2 weighs an approximate 2284.14 kg. This is much higher than the estimated propulsion system weight of 1600 kg. This means that the payload needs to be reduced significantly to accommodate the propulsion system. Although the weight is much higher than expected, the collective results of the subgroups bring a functioning, efficient and safe all-electric aircraft propulsion system.

6.2. Intragroup Results

In the end, the energy storage, wiring design and safety considerations, overall safety measures for arcing and partial discharge have been discussed as well as methods to mitigate the destructive thermal runaway. In accordance to the requirements given in the program of requirements, as stated in Chapter 2, the following research and design choices have been fulfilled:

- **Battery Design and Architecture:**
  - Battery cells based on Li-S technology with an energy density of 600-650 Wh/kg have been used to power the plane.
  - Two battery systems comprised of 4 battery packs are used for a total embedded power of 2 MW per battery system.
  - The BESS provides enough energy to fly the required mission length of 260km (50 km inclusive) using given power requirements.
  - The energy storage system has a total energy capacity of 562 kWh.

  - The total weight of the BESS is 1067 kg.
  - With safety in mind, a backup battery is used that can power only the avionics for 16 minutes.
  - The battery has a BMS that monitors and protects the battery pack using SoC, SoH, voltage/current monitoring and equalised cell charging.
  - Thermal runaway has been discussed and prevention techniques have been chosen for the design.

- **Wiring System:**
  - The rules of conductor sizing are given and supported by simulation plots.
  - A temperature analysis is provided as a hypothesis of the temperature in the cable.
  - Table 4.2 shows the dimensions of the cable conductor and their respective properties.
  - The total estimated weight for the wiring system is 284.54 kg.
  - Connectors were selected based on the type of connection that needed to be made, also including safety considerations.

- **High Voltage Considerations:**
  - Different layers of a high-voltage cable were looked at and how they help prevent partial discharge.
  - Table 5.2 shows the insulation thicknesses for the different cables used in the electrical architecture.
  - Cables are equipped with a semiconductor layer which is 1.2 mm thick and a shield layer which is 2 mm thick.
  - Parallel & series arcing has been discussed and detection methods combined with protection components to mitigate them are given.

6.3. Overall Reflection

6.3.1. Battery Design and Architecture

For the battery technology, a couple of specifications regarding the reliability of the system are missing, as it is hard to predict that in the future. Consequently, other technologies such as Li-air and Solid-State batteries could have gotten more research to look into the feasibility of these batteries and if their development would actually take that predicted time. If more concrete evidence were to be found into their future aspects, these technologies would have been chose to reduce the total weight of the battery pack as less cells would be needed. All in all, based on the information available today, we are content with the choice of Li-S battery cells.
For the thermal runaway mitigation, plenty of techniques and electronic mitigation techniques have been discussed and presented. However, a more in-depth view in how these work combined with a more detailed look in the specific components and their weight would be desired to get a better mass estimation.

6.3.2. Wiring System

All in all the wiring system has received a lot of consideration, however, the weight of the wire could be quite far off of what an actual aircraft of this size might look like. The reason for this is because a lot of assumptions were made while in reality these assumptions and estimations might not hold or be quite inaccurate. Generally the wire lengths look like they could be an over estimation of the length, which means the weight described in the results could be a lot larger than it actually will be should this aircraft be built. All the design decisions were also based on the length, for example, all of the temperature dissipation is a function of the length ($A = 2\pi \cdot r \cdot l$). This means that, inherently, all of the simulations also carry a large error margin. Perhaps it would have also been desirable to present actual commercially available connectors to help illustrate the design choices there.

6.3.3. High Voltage Considerations

Regarding partial discharges, it was assumed that the semiconducting layer and the shield layer would be the same for all voltage levels while these thicknesses were selected at the highest voltage level to be sure that the entire system would be safer as a whole. In actuality the thickness should change as

a function of the voltage, current and conductor radius. The conductor thickness would not have a too large effect on the overall weight of the cable system but the shield thickness can potentially reduce the weight by a significant margin.
Regarding series and parallel arcing, a comparison between several detection methods would have given a better overview why a certain method has been chosen over another one. Again, a deeper dive into actual real-world components that could be used in the plane would have given a greater insight regarding weight and workings of these components. This, combined with a more detailed explanation into the workings of these components would have been preferred, but felt out of the scope of this thesis.

7

Conclusion & Future Work

7.1. Conclusion

The goal of this thesis was to provide an estimate of what the battery energy storage system and the cabling might look like in an electric aircraft. Furthermore, this was also meant to discuss high-voltage phenomena and how they are relative to an electric aircraft flying at high altitudes. The energy requirements were found based on the requested electrical power described in the program of requirements which allowed a prediction to made of the architecture of the BESS. The number of series and parallel modules were found including the number of series and parallel cells per module. A discussion of the cell technology was made which lead to the decision of using lithium-sulfur cell technology because of its promising energy density and high probability of availability by 2038. Methods to prevent thermal runaway from occurring were discussed and an estimate was made of the weight of the thermal runaway mitigation system which includes the battery management system. An estimation was then made of the total weight of the battery system, using this the battery level energy density was calculated.
The different rules for the sizing of conductors and insulation were discussed, which lead to a prediction in the design of different cables that could be used in the electrical architecture. The different layers of cables were looked at and why they are necessary in the high-voltage system. To this end the phenomenon of partial discharges was discussed and how the aforementioned layers help prevent this phenomenon from occurring. To finish off the electrical transportation system, components were selected to help prevent arcing in the entire system. Combining all of the above mentioned electrical components and systems provides a design concept for how to store and distribute electrical energy throughout a fully electric aircraft.

7.2. Future Work

If this project were to continue into the future a more detailed design could be implemented. In this thesis only one cell technology was actually used in the implementation of the propulsion system. The other cells can also be used to design a battery and a comparison of the different battery systems can be made and their viability can be further explored. Thermal runaway mitigation can also be further explored through looking at how the technology for removing heat will improve before the year 2038 and how it affects the battery system weight. More research could be done into specifics regarding the thermal runaway mitigation components to get a more accurate view of safety and weight in this system. In this thesis the cable semiconducting layer and shield layer thicknesses are taken as constant in order to keep the system as safe as possible, however, these thicknesses should decrease with voltage level and change as a function of the radius of the rest of the cable, which could be looked into in the future. Lastly, for partial discharge mitigation and arc mitigation, further research can be done into also localising the partial discharges and arcs so that these areas can be isolated. This increases the safety of the system as a whole as knowing where partial discharges occur give a hint at which cables need to be checked more often than others. Furthermore, the localisation of arcs can help with diagnostics and repair of electrical systems. More components regarding these issues could be studied and compared as well as going in-depth into future possibilities.

Bibliography

[1] *Encyclopedia of Electrochemical Power Sources*. Elsevier Science, 2009.

[2] Lorenzo Grande et al. “The Lithium/Air Battery: Still an Emerging System or a Practical Reality?” In: *Advanced Materials* 27.5 (2015), pp. 784–800. DOI: https://doi.org/10.1002/adma.201403064.

[3] Won-Jin Kwak et al. “Lithium–Oxygen Batteries and Related Systems: Potential, Status, and Future”. In: *Chemical Reviews* 120.14 (2020), pp. 6626–6683. DOI: 10.1021/acs.chemrev.9b00609.

[4] N. Imanishi and O. Yamamoto. “Perspectives and challenges of rechargeable lithium–air batteries”. In: *Materials Today Advances* 4 (2019), p. 100031. ISSN: 2590-0498. DOI: https://doi.org/10.1016/j.mtadv.2019.100031.

[5] R. Marc. “Solid-state batteries inch their way to market”. In: *Chemical and Engineering News* 95 (Nov. 2017), pp. 19–21. DOI: 10.1021/cen-09546-bus.

[6] K. Hideyuki et al. “Extremely Low Resistance of Li3PO4 Electrolyte/Li(Ni0.5Mn1.5)O4 Electrode Interfaces”. In: *ACS Applied Materials & Interfaces* 10.32 (2018), pp. 27498–27502. DOI: 10.1021/acsami.8b08506.

[7] Oxis Energy. *Our Cell and Battery Technology Advantages*. URL: https://oxisenergy.com/technology/ (visited on 06/03/2022).

[8] L. Blain. “Super-dense lithium-sulfur battery gives electric plane a 230-mile range”. In: *New Atlas* (2020). [Online, accessed 05-06-2022]. URL: https://newatlas.com/aircraft/oxis-lithium-sulfur-battery-electric-aircraft/.

[9] I. Buchmann. *Batteries in a Portable World: A Handbook on Rechargeable Batteries for Non-Engineers*. 3rd ed. Cadex Electronics Inc., 2011.

[10] Cessna By Textron Aviation. *Citation CJ4 Gen2*. URL: https://cessna.txtav.com/en/citation/cj4-gen2 (visited on 06/06/2022).

[11] IEEE. *IEEE/AIAA ITEC+EATS Student Design Challenge - IEEE Transportation Electrification Community*. 2022. URL: https://tec.ieee.org/conferences-workshops/2022-ieee-aiaa-itec-eats-student-design-challenge (visited on 05/31/2022).

[12] N. Fontenai and R. de Graaff. “Design of Propulsion System for 9 PAX Electric Aircraft - Motors and Power Distribution for AEA”. In: (2022).

[13] G. Junling and L. Jinping. “Binder-free electrode architecture design for lithium-sulfur batteries: A review”. In: *Nanoscale Advances* 1 (Apr. 2019). DOI: 10.1039/C9NA00040B.

[14] M. K. Eren et al. “Effects of Cell and Module Configuration on Battery System in Electric Vehicles”. In: *ENGINEERING TECHNOLOGIES-IJET* 4.4 (2018).

[15] Z. Chenxi, Y. Huigen, and L. Hong. “Enabling the thermal stability of solid electrolyte interphase in Li-ion battery”. In: *InfoMat* 3.6 (2021), pp. 648–661. DOI: https://doi.org/10.1002/inf2.12190. URL: https://onlinelibrary.wiley.com/doi/abs/10.1002/inf2.12190.

[16] John Revill. “Tesla crash may have triggered battery fire: Swiss firefighters”. In: *Reuters Technology News* (2018). URL: https://www.reuters.com/article/us-swiss-tesla-crash-idUSKCN1IF2WN (visited on 05/14/2018).

[17] REUTERS/Rescue Media. *An electric-powered Tesla car burns after a crash on the Swiss A2 motorway on Monte Ceneri near Bellinzona*. [Online, accessed 05-06-2022]. 2018. URL: https://www.reuters.com/article/us-swiss-tesla-crash-idUSKCN1IH25G.

[18] Dragonfly Energy. “Thermal Runaway”. In: (2021). URL: https://dragonflyenergy.com/thermal-runaway/ (visited on 04/21/2021).

[19] L. Huang et al. “Thermal runaway routes of large-format lithium-sulfur pouch cell batteries”. In: *Joule* 6.4 (2022), pp. 906–922. ISSN: 2542-4351. DOI: https://doi.org/10.1016/j.joule.2022.02.015. URL: https://www.sciencedirect.com/science/article/pii/S2542435122000964.

[20] Z. Liao et al. “A survey of methods for monitoring and detecting thermal runaway of lithium-ion batteries”. In: *Journal of Power Sources* 436 (2019), p. 226879. ISSN: 0378-7753. DOI: https://doi.org/10.1016/j.jpowsour.2019.226879. URL: https://www.sciencedirect.com/science/article/pii/S0378775319308729.

[21] X. Feng et al. “Mitigating Thermal Runaway of Lithium-Ion Batteries”. In: *Joule* 4.4 (2020), pp. 743–770. ISSN: 2542-4351. DOI: https://doi.org/10.1016/j.joule.2020.02.010. URL: https://www.sciencedirect.com/science/article/pii/S254243512030088X.

[22] H-S. Ryu et al. “Discharge behavior of lithium/sulfur cell with TEGDME based electrolyte at low temperature”. In: *Journal of Power Sources* 163.1 (2006). Special issue including selected papers presented at the Second International Conference on Polymer Batteries and Fuel Cells together with regular papers, pp. 201–206. ISSN: 0378-7753. DOI: https://doi.org/10.1016/j.jpowsour.2005.12.061. URL: https://www.sciencedirect.com/science/article/pii/S0378775306000565.

[23] X. Li et al. “Safe and Durable High-Temperature Lithium–Sulfur Batteries via Molecular Layer Deposited Coating”. In: *Nano Letters* 16.6 (2016). PMID: 27175936, pp. 3545–3549. DOI: 10.1021/acs.nanolett.6b00577. eprint: https://doi.org/10.1021/acs.nanolett.6b00577. URL: https://doi.org/10.1021/acs.nanolett.6b00577.

[24] Z. Zhou et al. “Wide Working Temperature Range Rechargeable Lithium–Sulfur Batteries: A Critical Review”. In: *Advanced Functional Materials* 31.50 (2021), p. 2107136. DOI: https://doi.org/10.1002/adfm.202107136. eprint: https://onlinelibrary.wiley.com/doi/pdf/10.1002/adfm.202107136. URL: https://onlinelibrary.wiley.com/doi/abs/10.1002/adfm.202107136.

[25] S. Hemavathi. “Overview of cell balancing methods for Li-ion battery technology”. In: *Energy Storage* 3.2 (2021), e203. DOI: https://doi.org/10.1002/est2.203. eprint: https://onlinelibrary.wiley.com/doi/pdf/10.1002/est2.203. URL: https://onlinelibrary.wiley.com/doi/abs/10.1002/est2.203.

[26] W-Y. Chang. “The state of charge estimating methods for battery: A review”. In: *International Scholarly Research Notices* 2013 (2013).

[27] N. Shateri et al. “Lithium-Sulfur Cell State of Charge Estimation Using a Classification Technique”. In: *IEEE Transactions on Vehicular Technology* 70.1 (2021), pp. 212–224. DOI: 10.1109/TVT.2020.3045213.

[28] A. Fotouhi et al. “Lithium-Sulfur Battery Technology Readiness and Applications—A Review”. In: *Energies* 10.12 (2017). ISSN: 1996-1073. DOI: 10.3390/en10121937. URL: https://www.mdpi.com/1996-1073/10/12/1937.

[29] N. Shateri et al. “An Experimental Study on Prototype Lithium–Sulfur Cells for Aging Analysis and State-of-Health Estimation”. In: *IEEE Transactions on Transportation Electrification* 7.3 (2021), pp. 1324–1338. DOI: 10.1109/TTE.2021.3059738.

[30] PushEVs. *EV Battery Specs*. 2020. URL: https://pushevs.com/ev-battery-specs/ (visited on 06/09/2022).

[31] Cea Tech. *A lightweight system to prevent thermal runaway in batteries*. 2022. URL: https://www.cea.fr/cea-tech/liten/english/Pages/Medias/News/Batteries/a-lightweight-system-to-prevent-thermal-runaway-in-batteries.aspx (visited on 06/09/2022).

[32] TIBTECH. *Metal properties comparison: electric conductivity, thermal conductivity, density, melting temperature*. 2018. URL: https://www.tibtech.com/conductivite.php?lang=en_US (visited on 05/31/2022).

[33] Eliot Aretskin-Hariton et al. “Power Cable Mass Estimation for Electric Aircraft Propulsion”. In: *AIAA AVIATION 2021 FORUM*. DOI: 10.2514/6.2021-3021. eprint: https://arc.aiaa.org/doi/pdf/10.2514/6.2021-3021. URL: https://arc.aiaa.org/doi/abs/10.2514/6.2021-3021.

[34] T. L. Bergman et al. *Fundamentals of Heat and Mass Transfer*. 7th ed. Hoboken, New Jersey: John Wiley Sons, Inc., 2011.

[35] M. G. Niasar. *TUDelft High voltage cable systems course: Lecture 3 - Cable accessories, cable ampacity, and cable installation*. 2022. URL: https://brightspace.tudelft.nl/d2l/le/content/400098/viewContent/2611837/View (visited on 06/23/2022).

[36] F. H. Kreuger. *Industrial High DC Voltage: 1. Fields, 2. Breakdowns, 3. Tests*. Delft, Netherlands: Delft University Press, 1995.

[37] Mide Technology Corporation | A Hutchinson Company. *Air Pressure at Altitude Calculator*. URL: https://www.mide.com/air-pressure-at-altitude-calculator (visited on 06/04/2022).

[38] T. W. Dakin et al. "Breakdown of Gases in Uniform Fields Paschen Curves for Nitrogen, Air and Sulfur Hexafluoride". In: *Electra* 32 (1974), pp. 61–82.

[39] F. C. Cheng. "Insulation thickness determination of polymeric power cables". In: *IEEE Transactions on Dielectrics and Electrical Insulation* 1.4 (1994).

[40] F. H. Kreuger. *Industrial High Voltage: 1. Electric fields, 2. Dielectrics, 3. Constructions*. Delft, Netherlands: Delft University Press, 1991.

[41] AWC Allied Wire & Cable. *Mil-Spec Aerospace Cable | Allied Wire and Cable*. URL: https://www.awcwire.com/mil-spec-aerospace (visited on 06/05/2022).

[42] W. Yanhui et al. "Research progress of semiconductive shielding layer of HVDC cable". In: *High Voltage* 5.1 (2020), pp. 1–6. DOI: https://doi.org/10.1049/hve.2019.0069. eprint: https://ietresearch.onlinelibrary.wiley.com/doi/pdf/10.1049/hve.2019.0069. URL: https://ietresearch.onlinelibrary.wiley.com/doi/abs/10.1049/hve.2019.0069.

[43] M. G. Niasar. *TUDelft High voltage cable systems course: Lecture 2 - Cable components and cable manufacturing*. 2022. URL: https://brightspace.tudelft.nl/d2l/le/content/400098/viewContent/2607411/View (visited on 06/05/2022).

[44] R. Paludo, G. C. da Silva, and V. S. Filho. "The study of semiconductor layer effect on underground cables with Time Domain Reflectometry (TDR)". In: *IOSR Journal of Electrical and Electronics Engineering* 7.6 (2013), pp. 01–07.

[45] J.-M. Meyer and A. Rufer. "A DC Hybrid Circuit Breaker With Ultra-Fast Contact Opening and Integrated Gate-Commutated Thyristors (IGCTs)". In: *Power Delivery, IEEE Transactions on* 21 (2006), pp. 646–651. DOI: 10.1109/TPWRD.2006.870981.

[46] H-K. Ji et al. "Optimal Design of a Band Pass Filter and an Algorithm for Series Arc Detection". In: *Energies* 11 (Apr. 2018), p. 992. DOI: 10.3390/en11040992.

[47] Electrical Technology. "AFCI: Arc Fault Circuit Interrupter. Types, Working & Applications". In: *Electrical Technology* (2021). [Online, accessed 05-06-2022]. URL: https://www.electricaltechnology.org/2021/09/afci-arc-fault-circuit-interrupter.html.

[48] M. Faifer et al. "A method for the detection of series arc faults in DC aircraft power networks". In: *2013 IEEE International Instrumentation and Measurement Technology Conference (I2MTC)*. 2013, pp. 778–783. DOI: 10.1109/I2MTC.2013.6555521.

[49] J. Brooks and G. Scott. "Arc-Fault Circuit Interrupters for Aerospace Applications". In: *Society of Automotive Engineers* (1999). [Online, accessed 05-06-2022]. URL: http://www.pyrogen.com/arcfaultsae99.pdf.

[50] M. Muniappan. "A comprehensive review of DC fault protection methods in HVDC transmission systems". In: *Protection and Control of Modern Power Systems* 6 (Dec. 2021). DOI: 10.1186/s41601-020-00173-9.

[51] Tandem Combination Type Arc-Fault Circuit Interrupters (CAFCI). Siemens. URL: https://assets.new.siemens.com/siemens/assets/api/uuid:6530acbf-5cf1-4c16-afa7-1af044796874/sie-ss-tandemcafci.pdf.

A Figures

A.1. Airplane Schematic

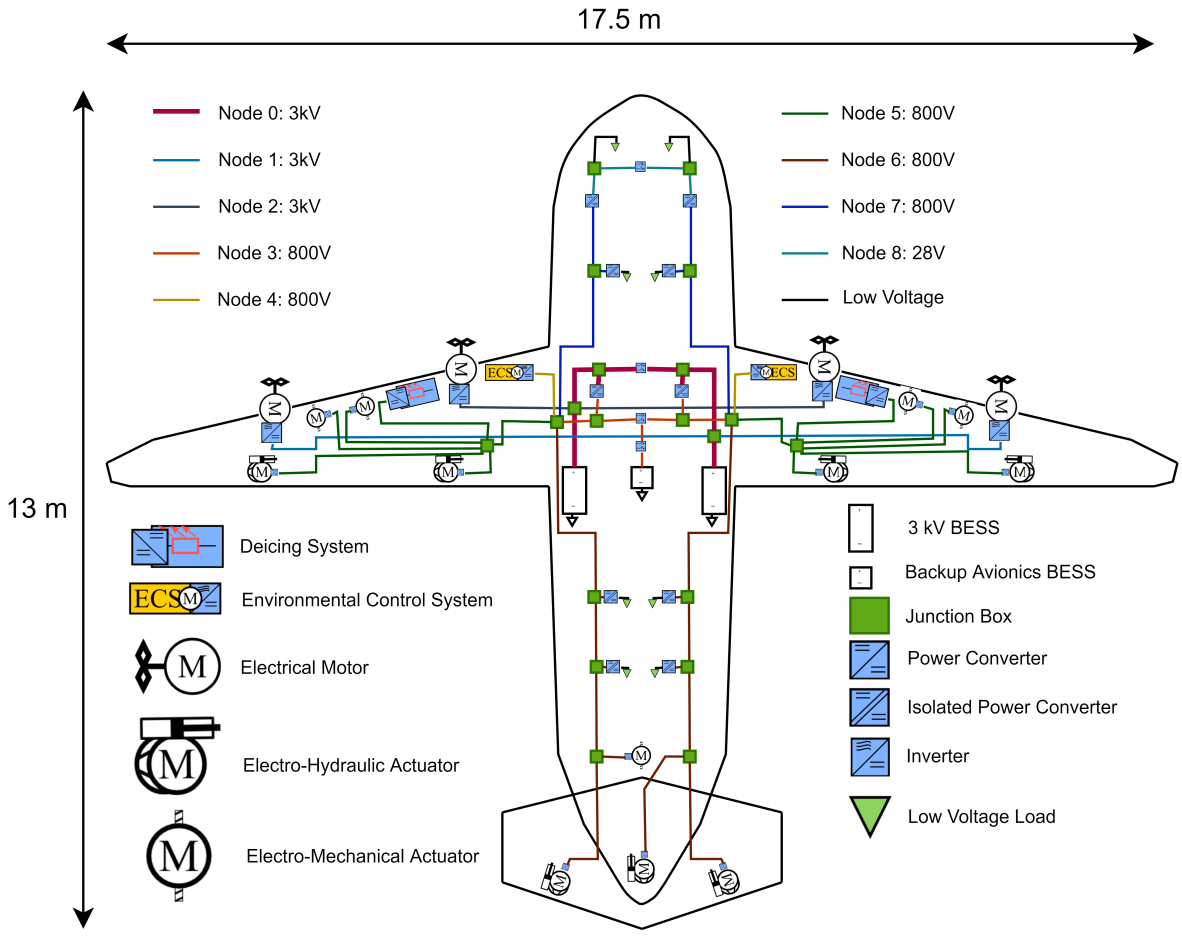

Figure A.1: Rough schematic of the airplane

A.2. Voltage Drops

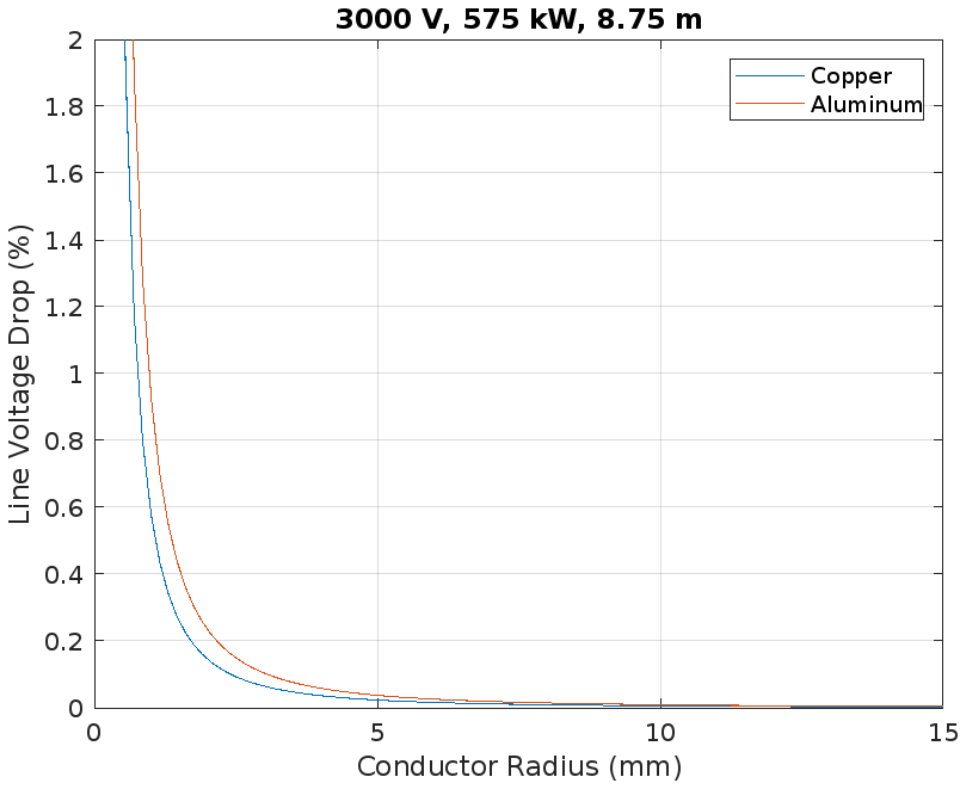

Figure A.2: Voltage drop as a function of conductor radius for Node 1

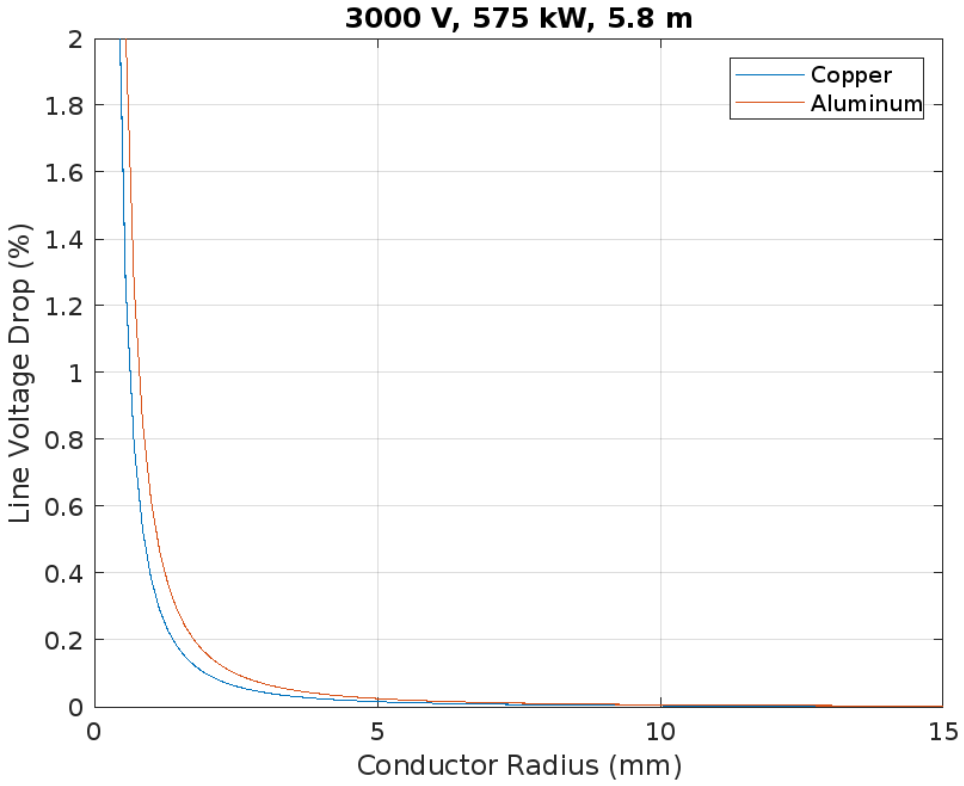

Figure A.3: Voltage drop as a function of conductor radius for Node 2

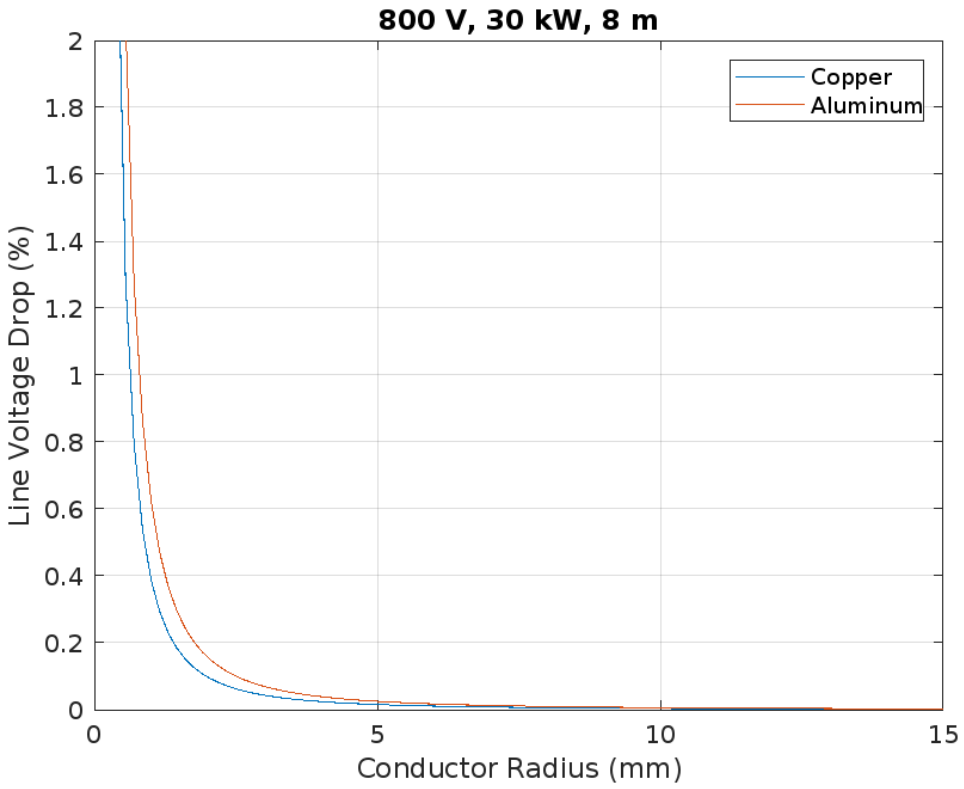

Figure A.4: Voltage drop as a function of conductor radius for Node 3

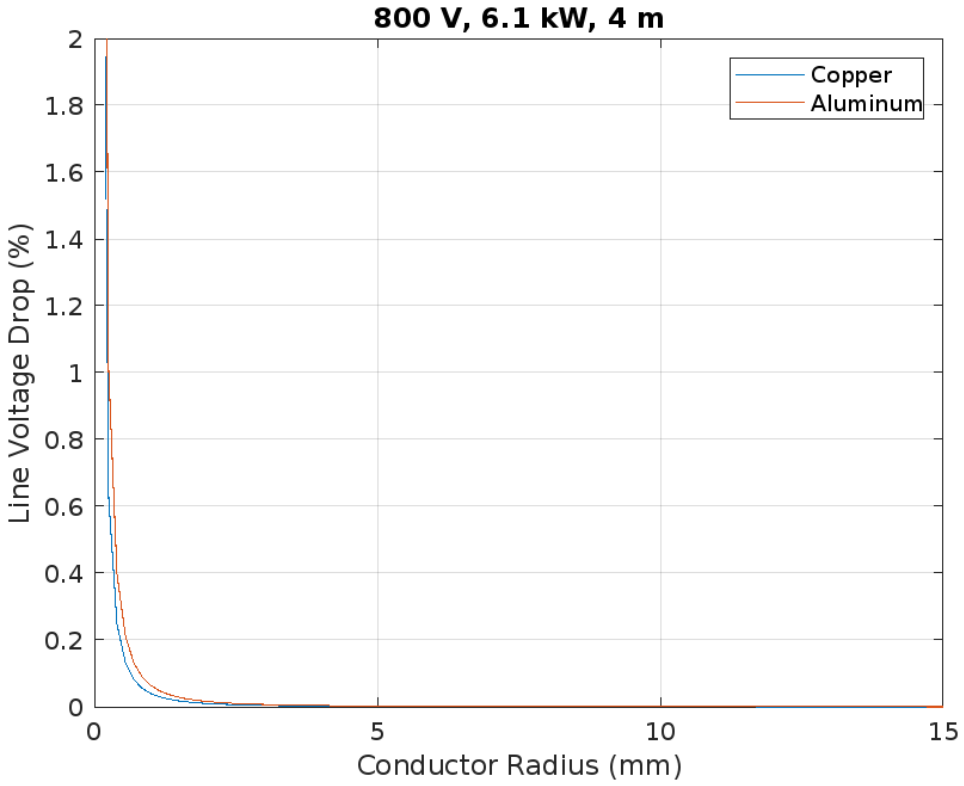

Figure A.5: Voltage drop as a function of conductor radius for Node 4

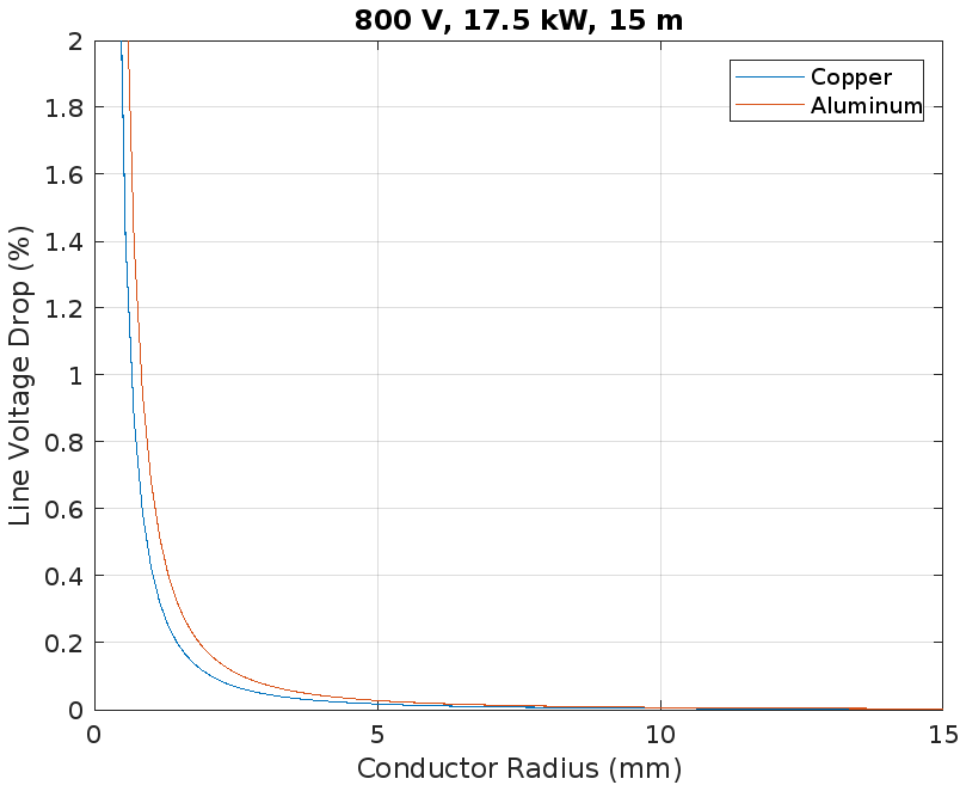

Figure A.6: Voltage drop as a function of conductor radius for Node 5

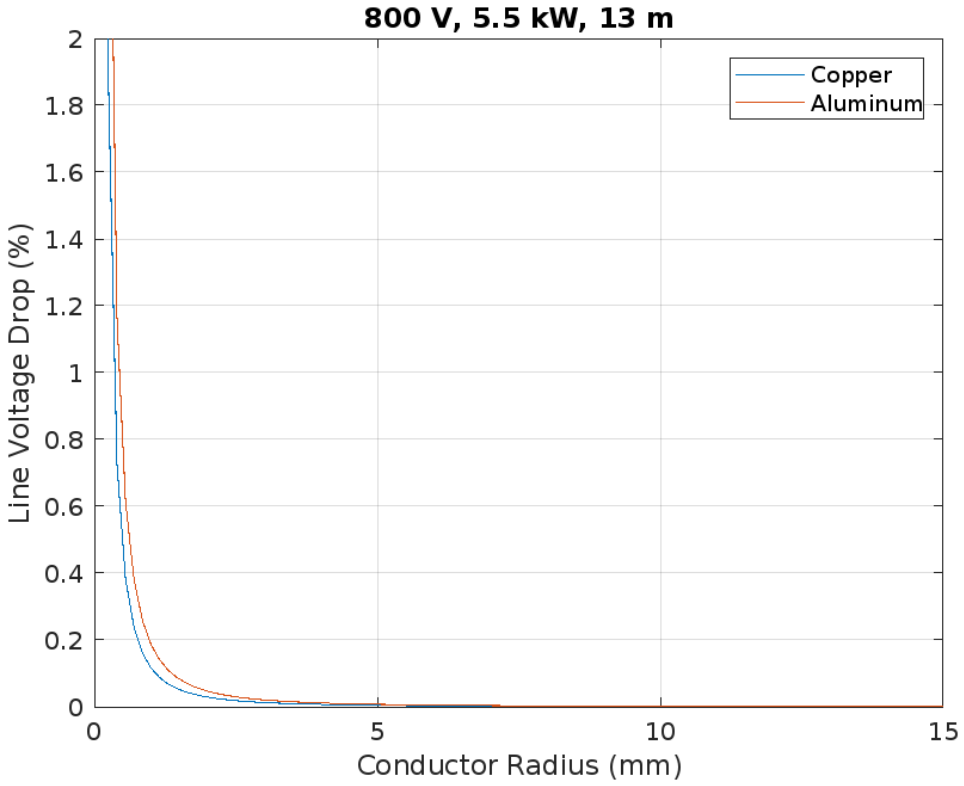

Figure A.7: Voltage drop as a function of conductor radius for Node 6

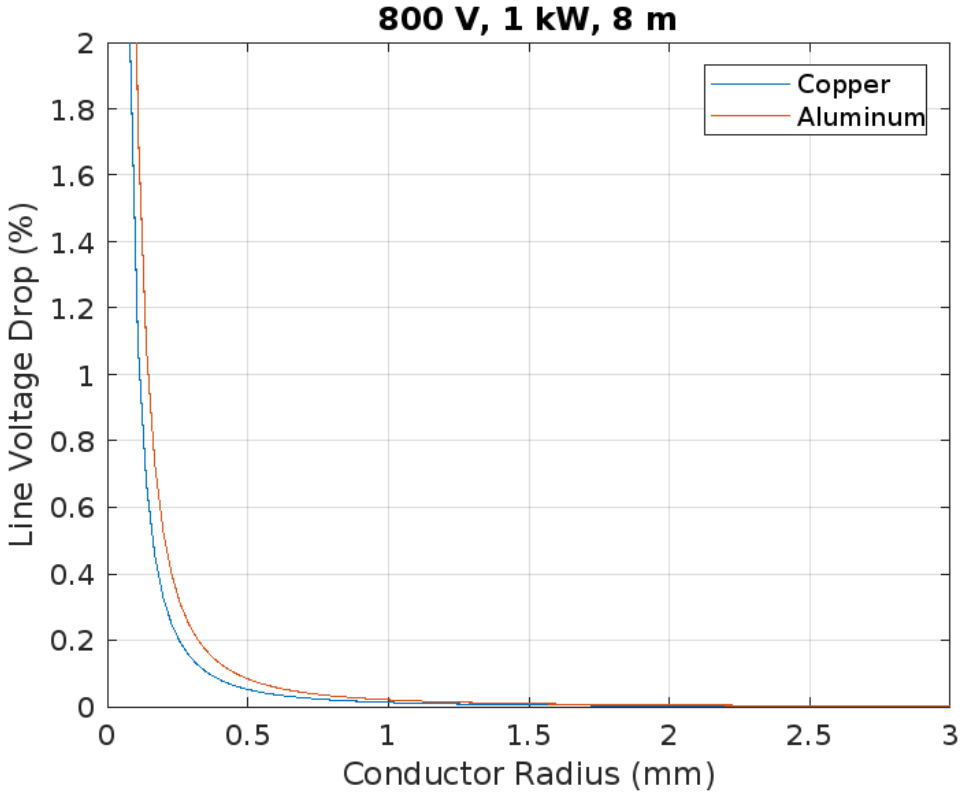

Figure A.8: Voltage drop as a function of conductor radius for Node 7

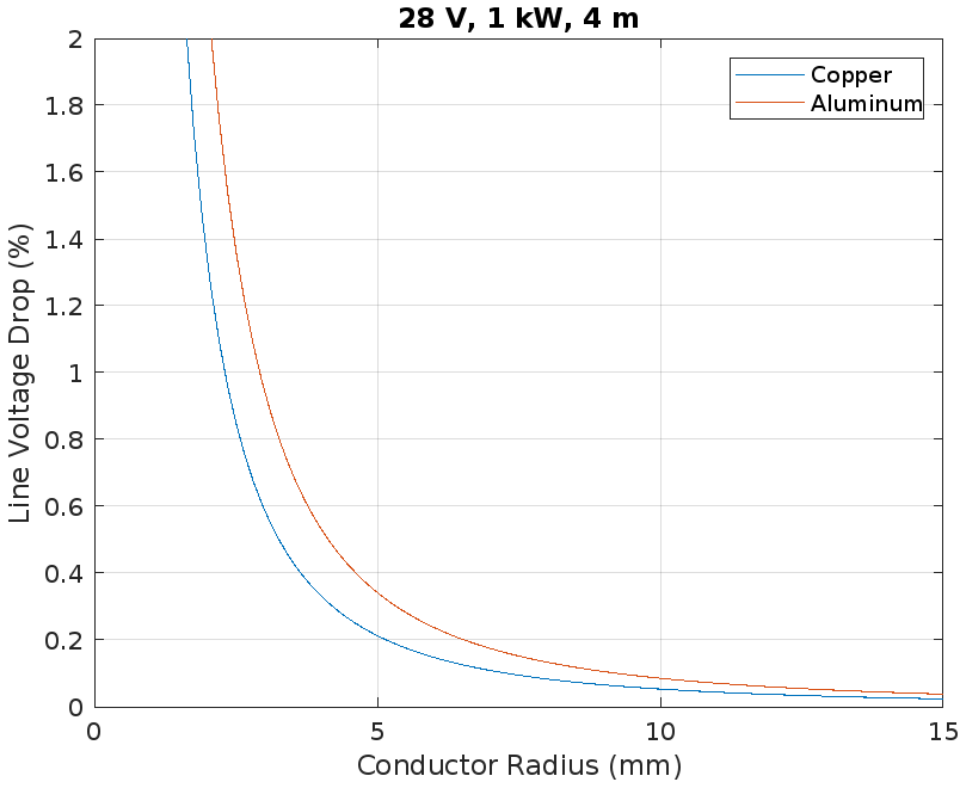

Figure A.9: Voltage drop as a function of conductor radius for Node 8

A.3. Wire Stead State Temperatures

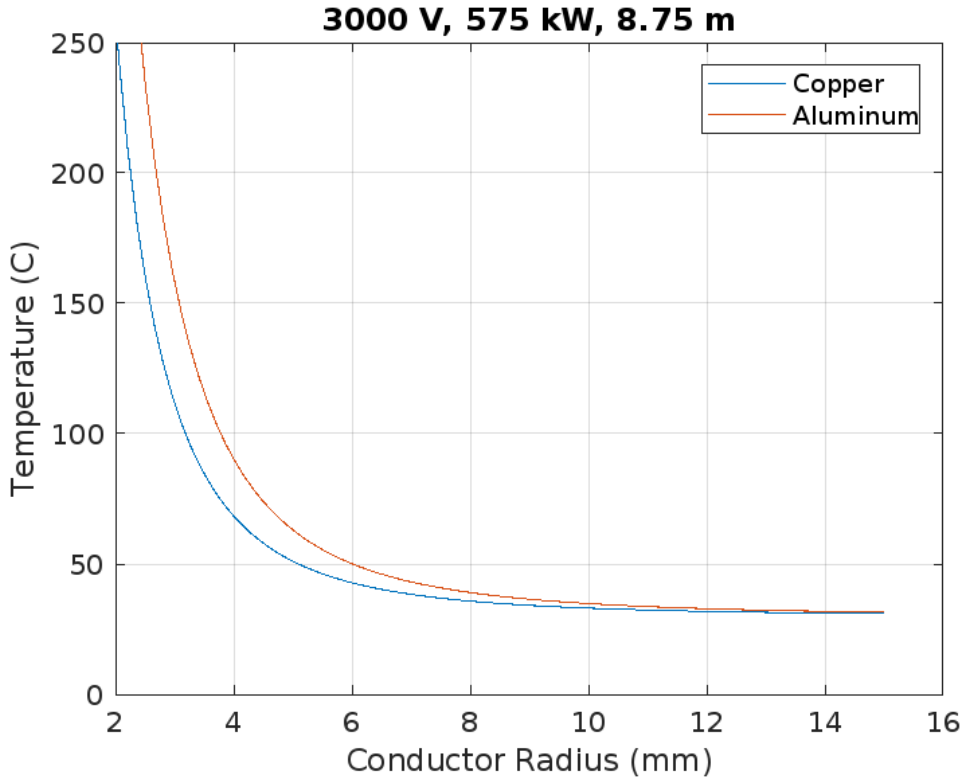

Figure A.10: Steady state temperature as a function of conductor radius for Node 1

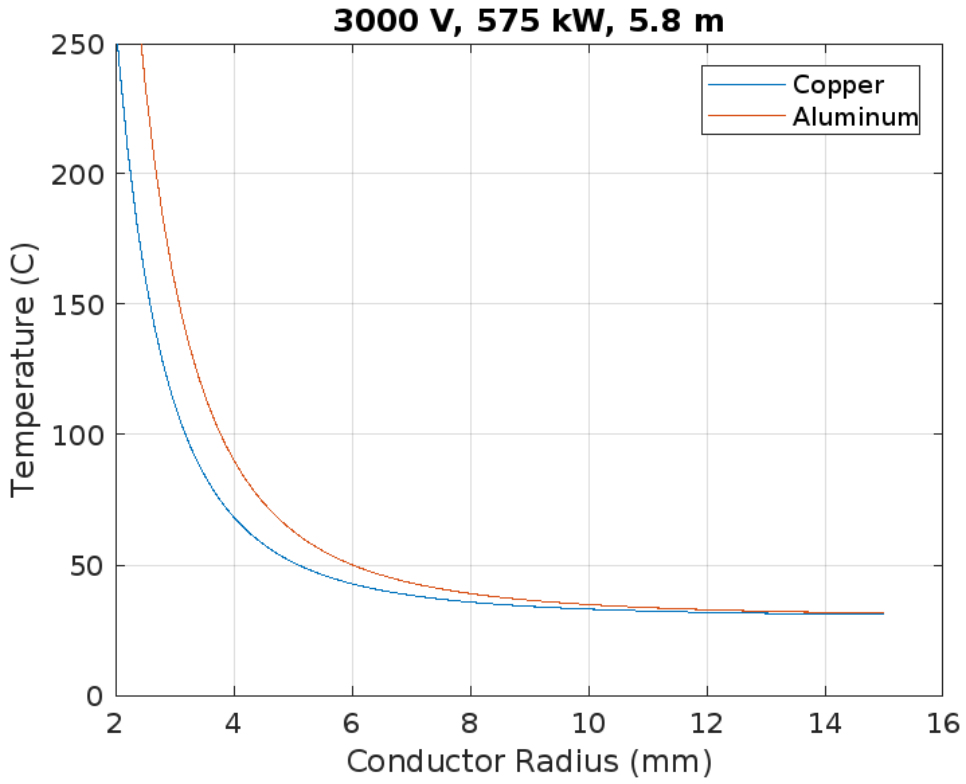

Figure A.11: Steady state temperature as a function of conductor radius for Node 2

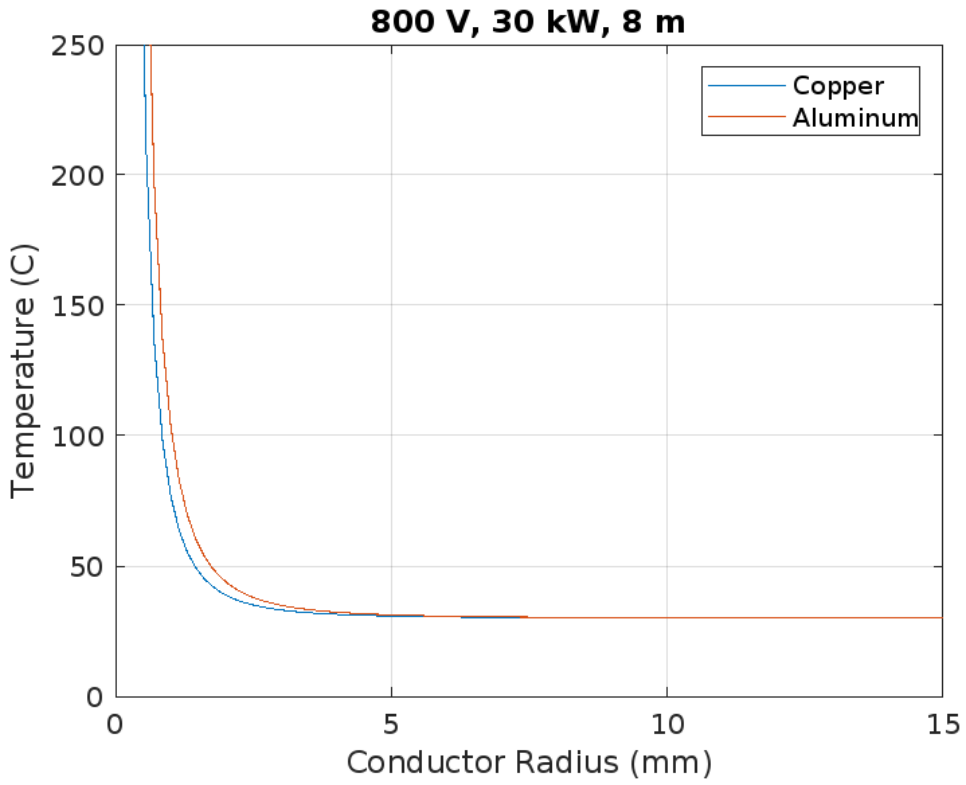

Figure A.12: Steady state temperature as a function of conductor radius for Node 3

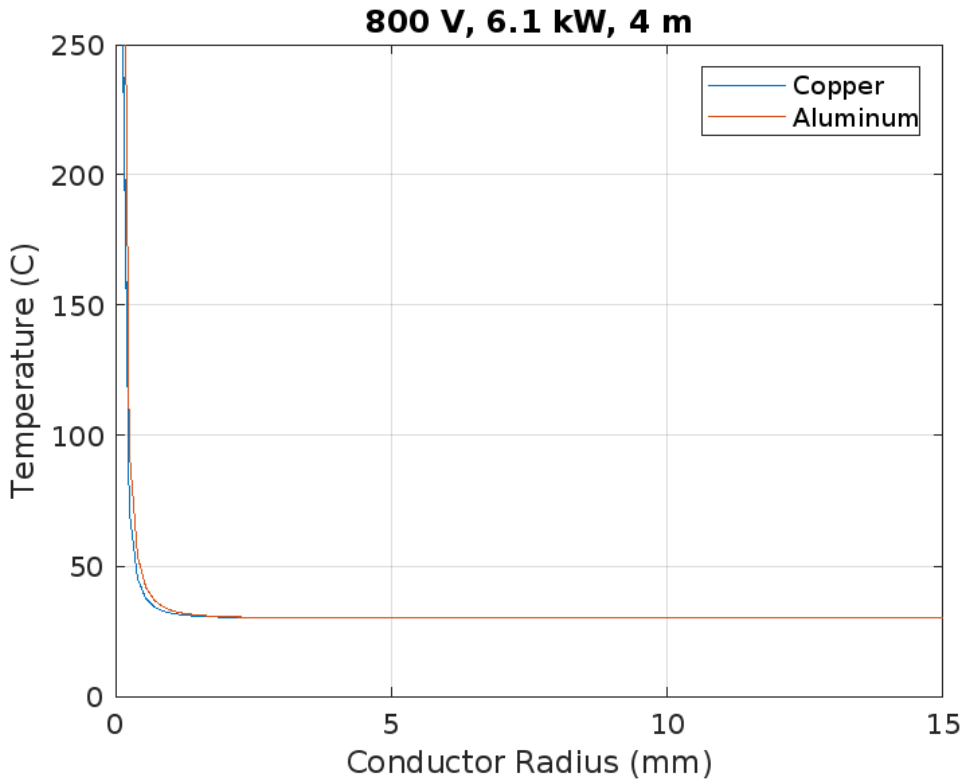

Figure A.13: Steady state temperature as a function of conductor radius for Node 4

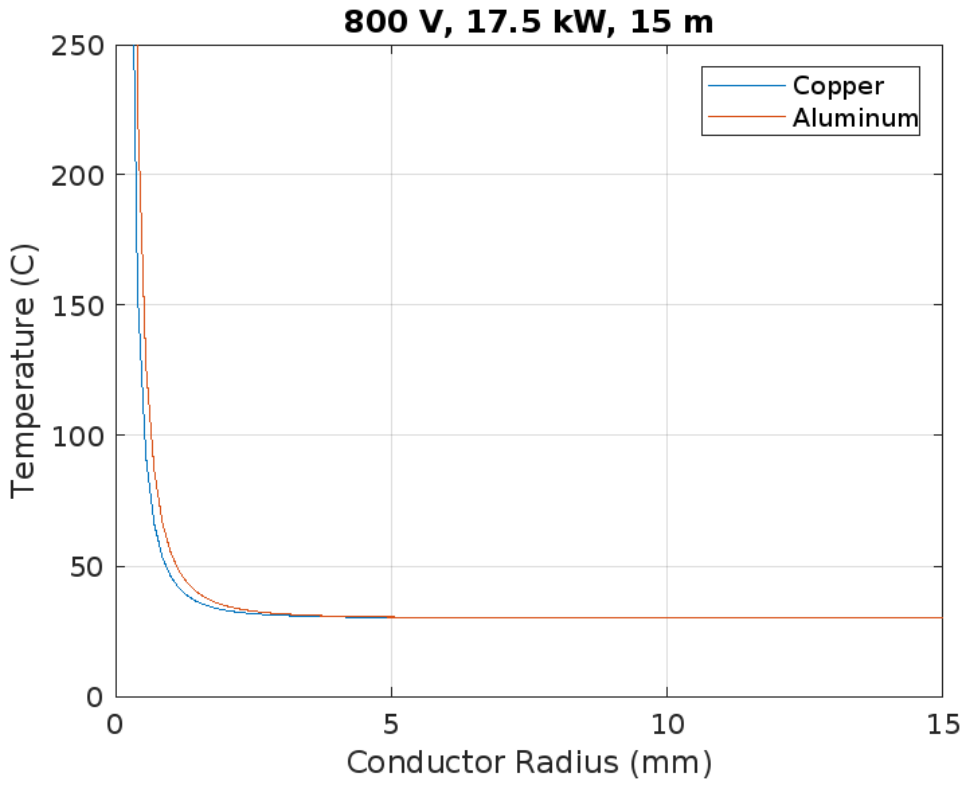

Figure A.14: Steady state temperature as a function of conductor radius for Node 5

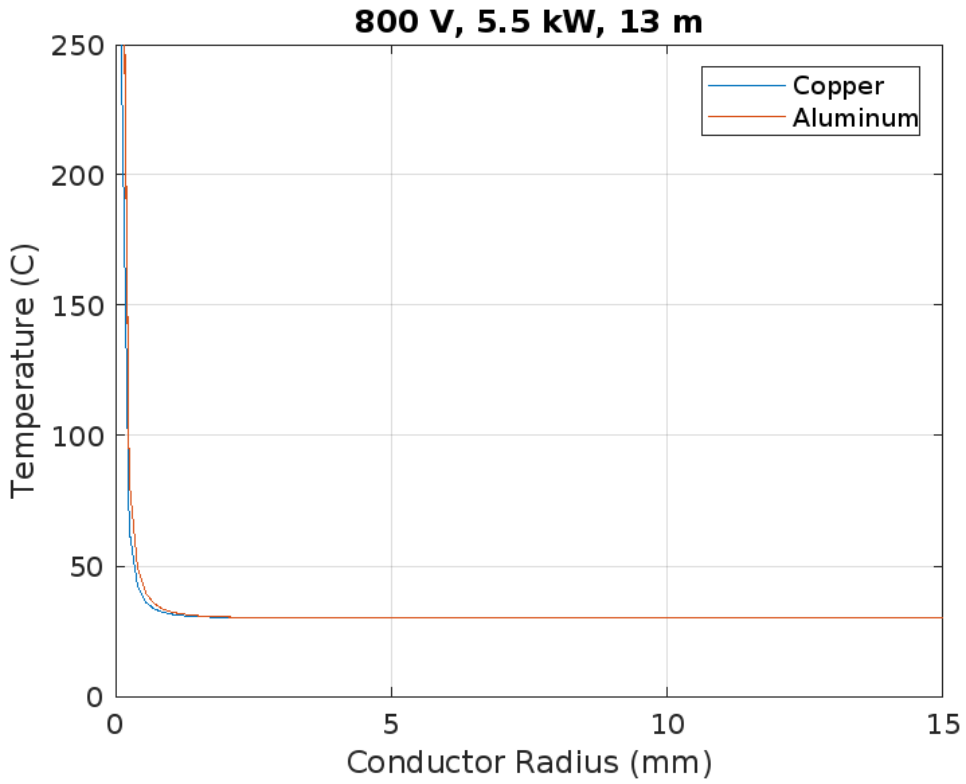

Figure A.15: Steady state temperature as a function of conductor radius for Node 6

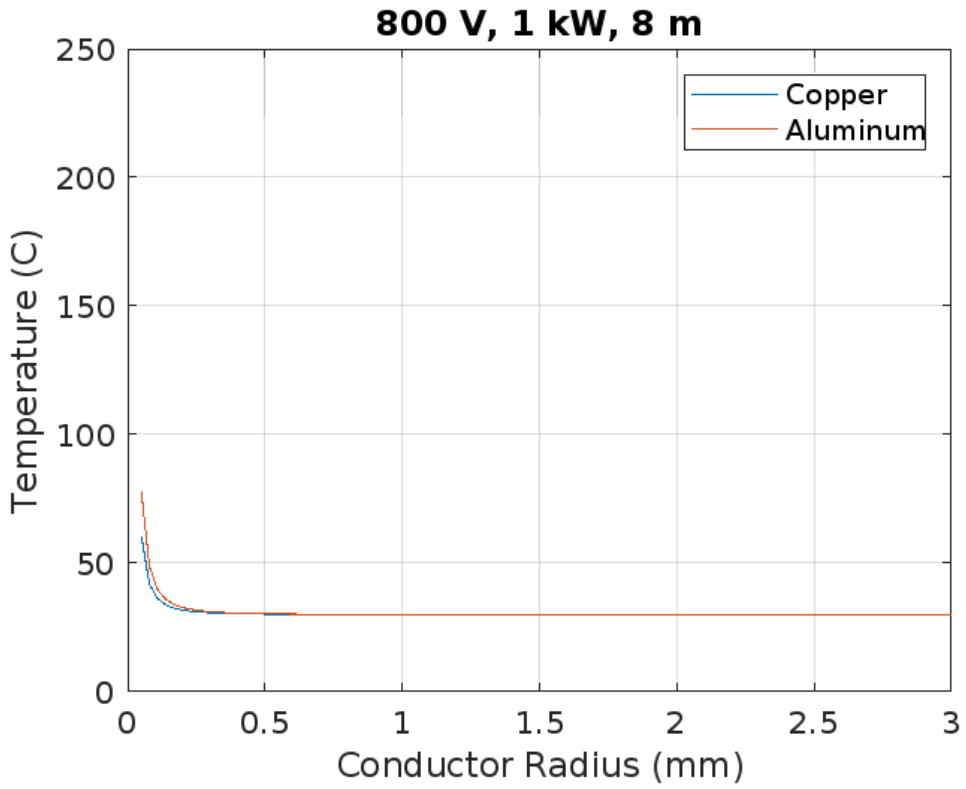

Figure A.16: Steady state temperature as a function of conductor radius for Node 7

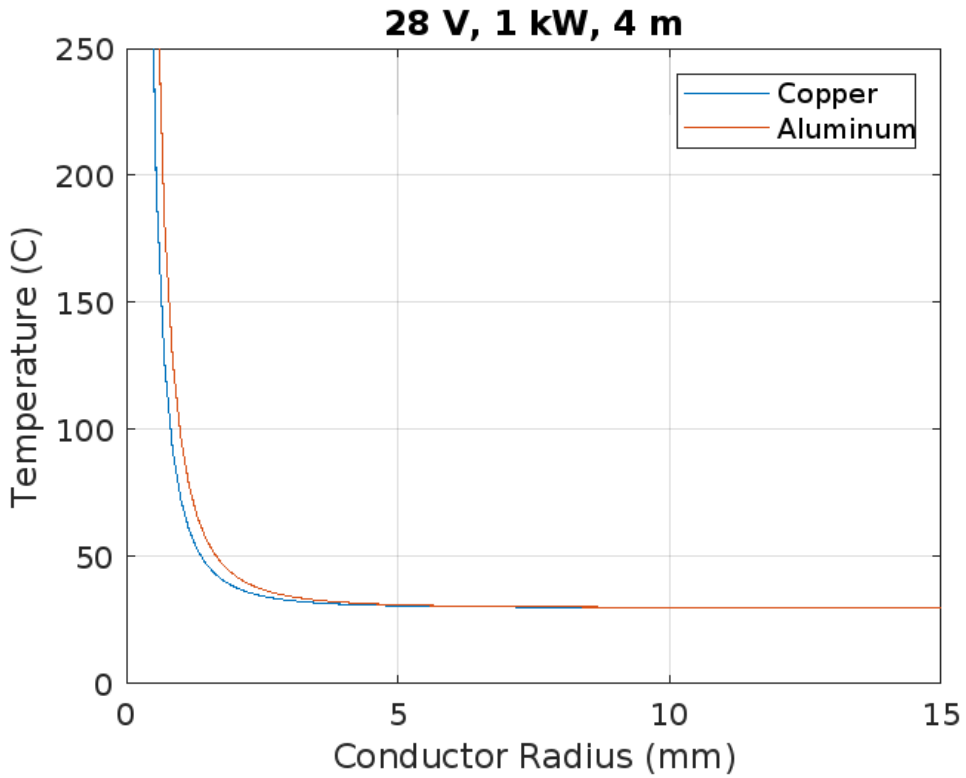

Figure A.17: Steady state temperature as a function of conductor radius for Node 8

A.4. Cable Masses

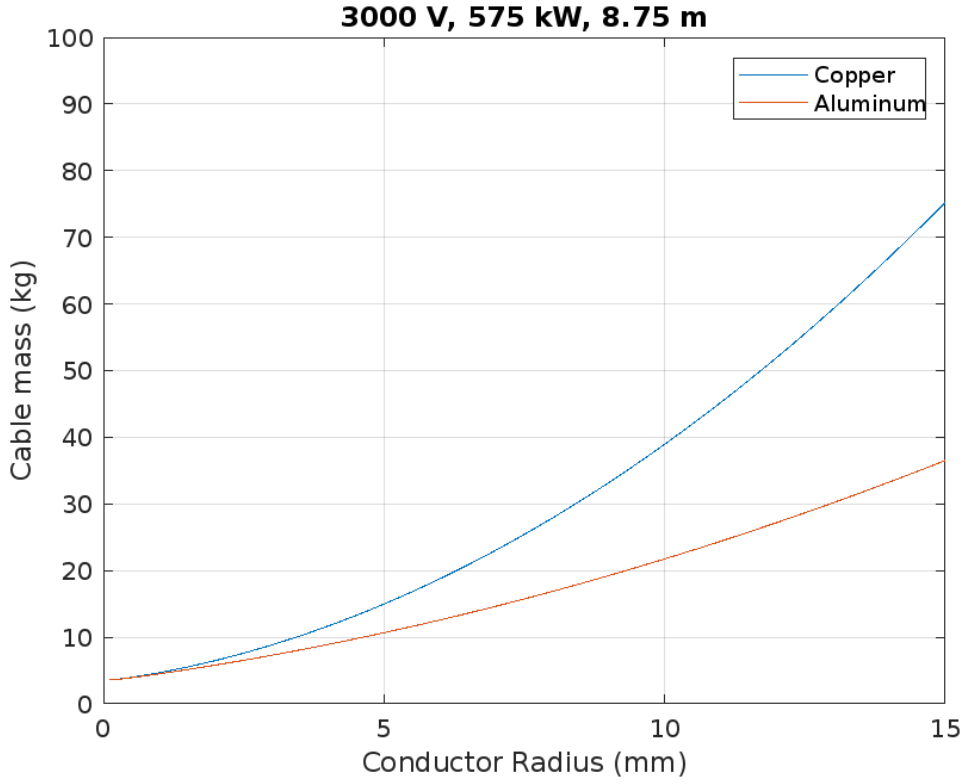

Figure A.18: Cable mass as a function of conductor radius for Node 1

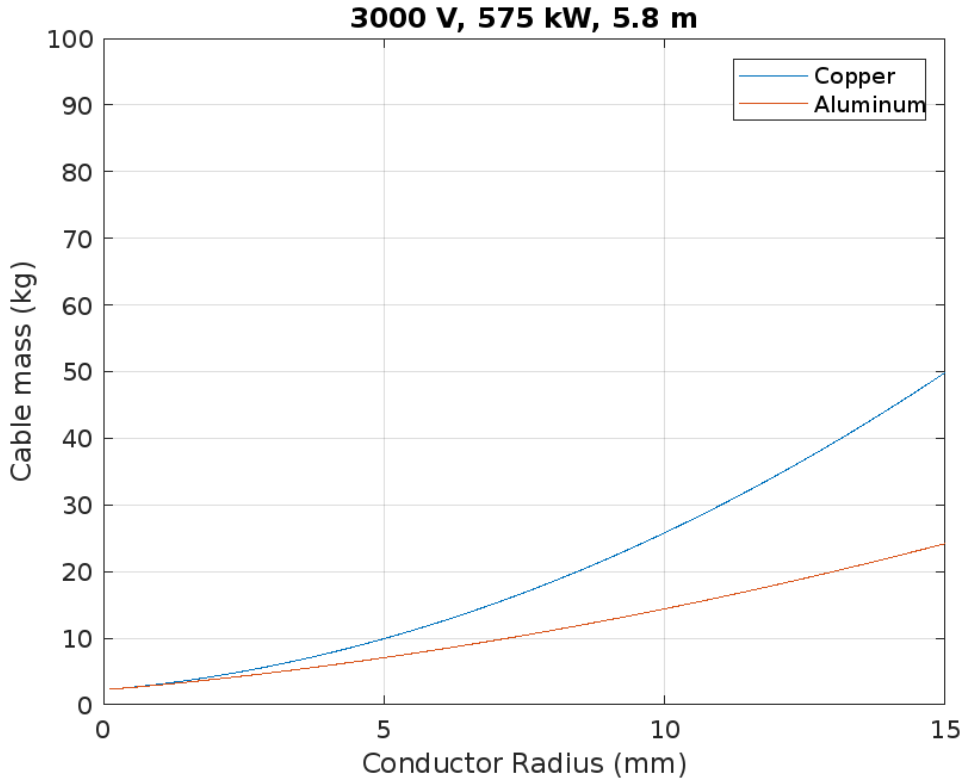

Figure A.19: Cable mass as a function of conductor radius for Node 2

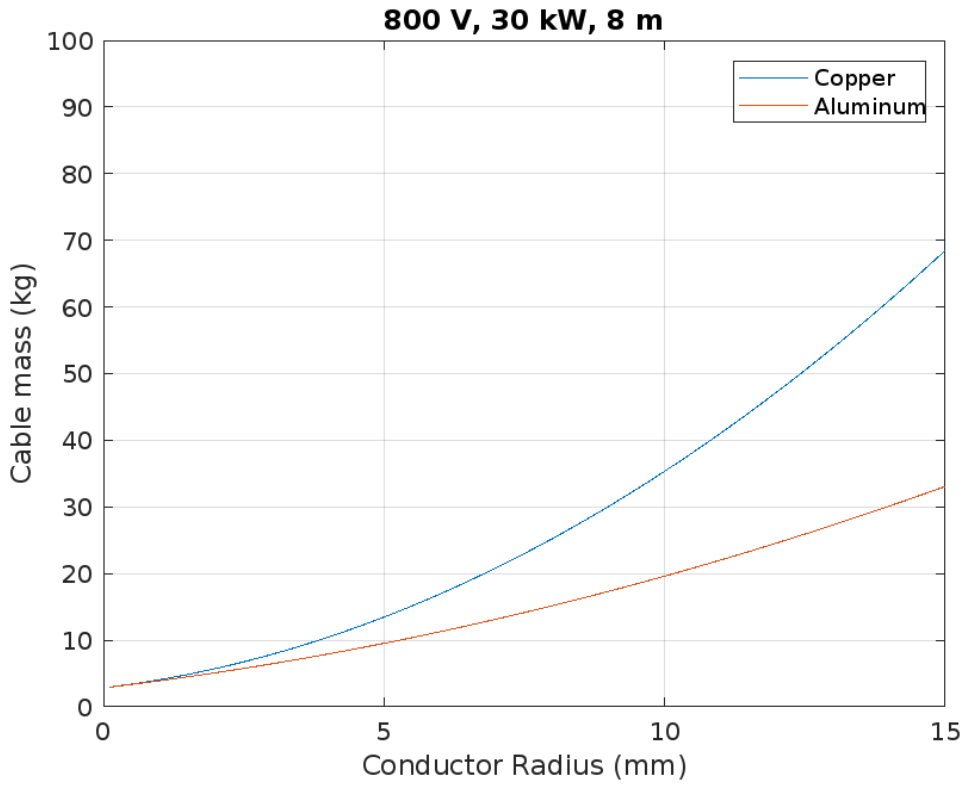

Figure A.20: Cable mass as a function of conductor radius for Node 3

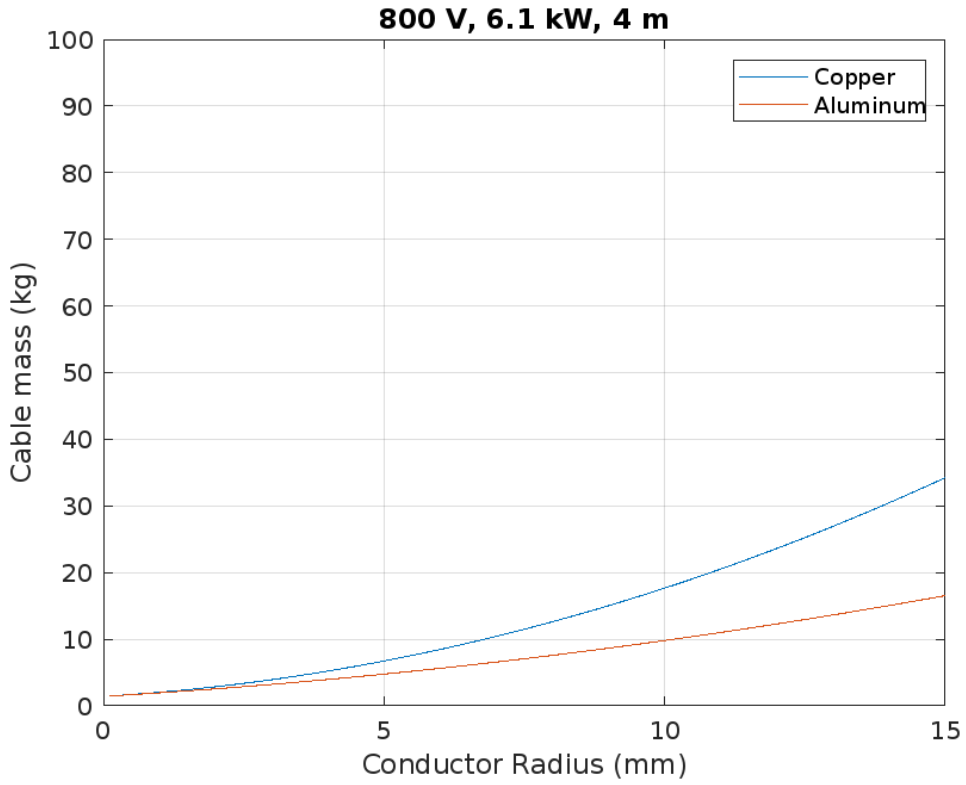

Figure A.21: Cable mass as a function of conductor radius for Node 4

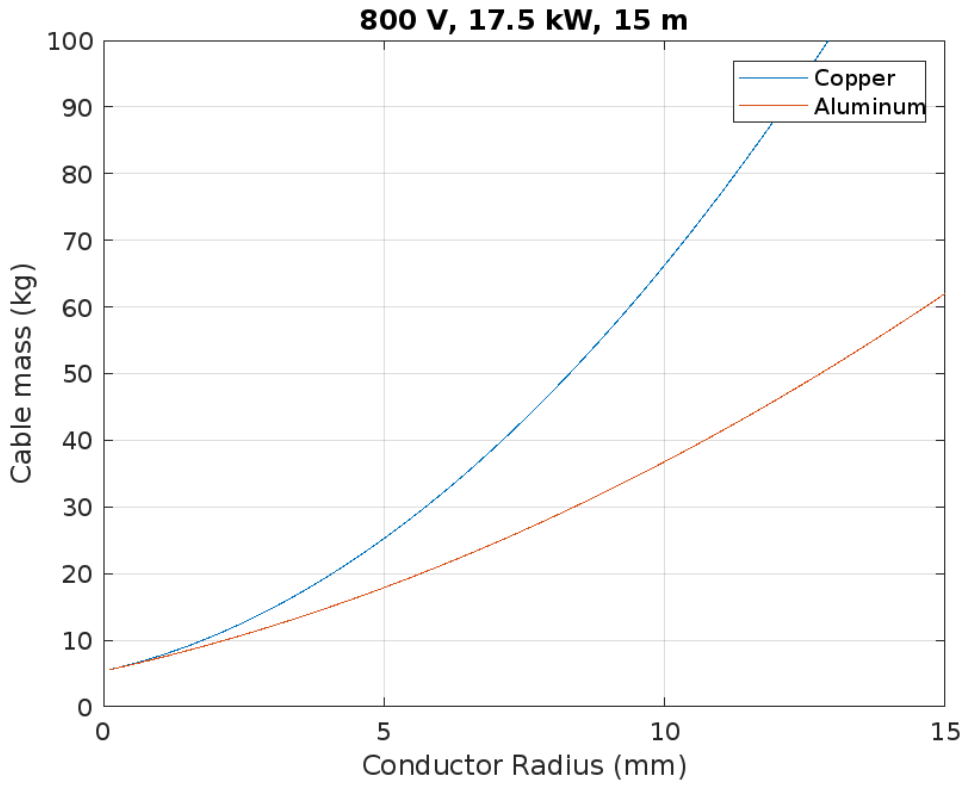

Figure A.22: Cable mass as a function of conductor radius for Node 5

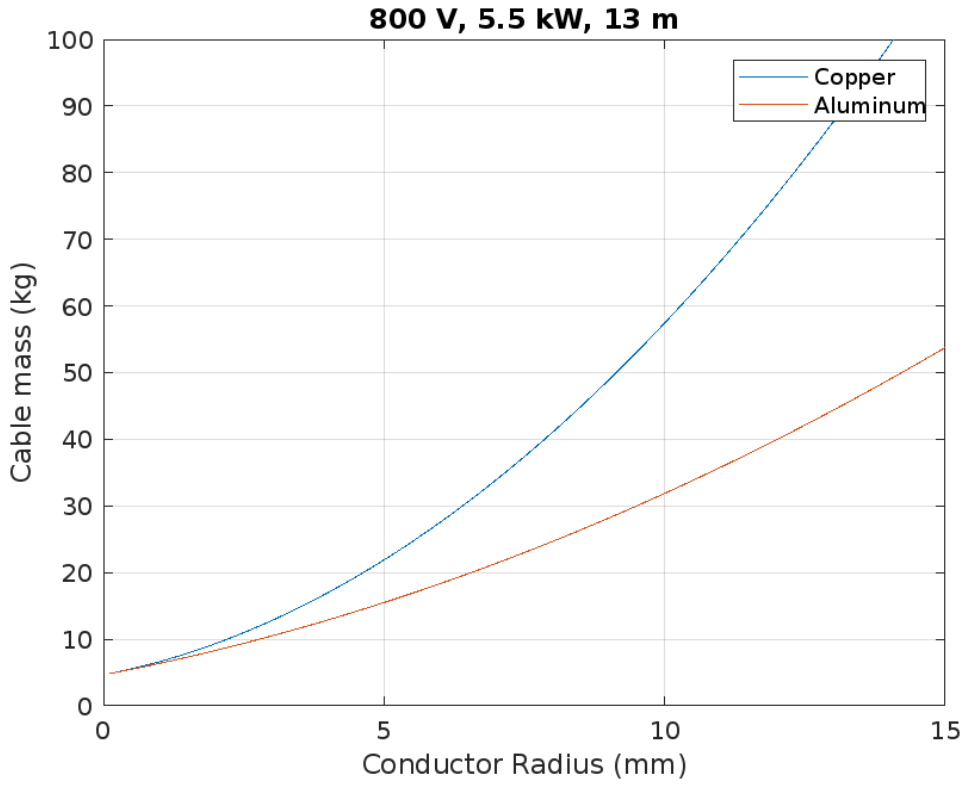

Figure A.23: Cable mass as a function of conductor radius for Node 6

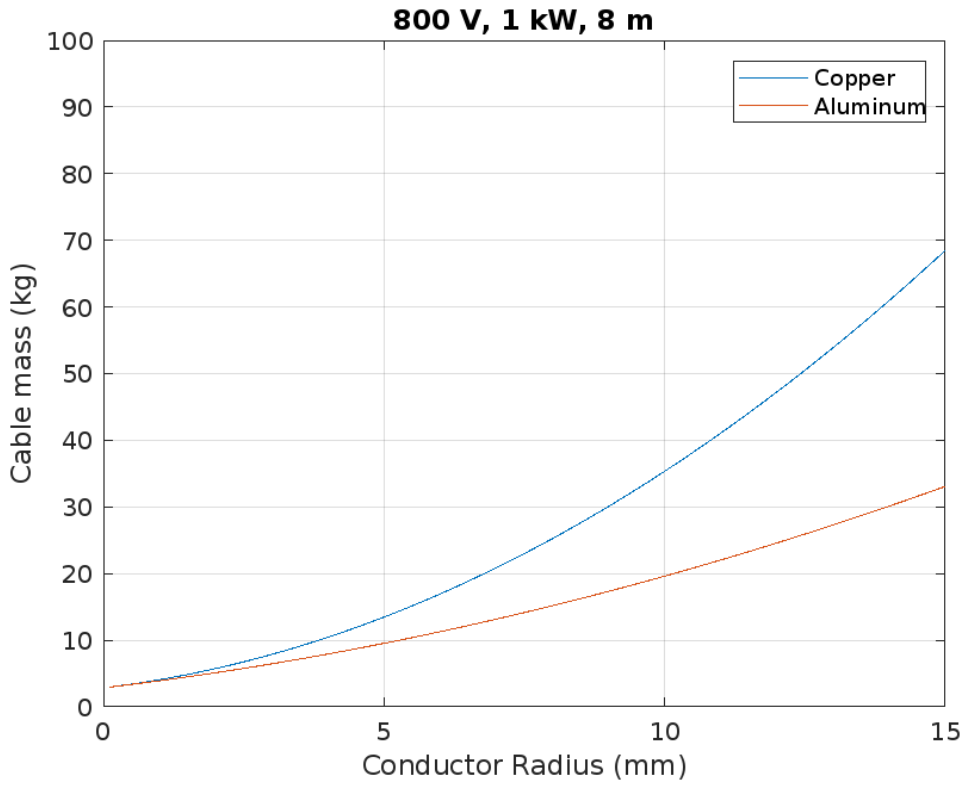

Figure A.24: Cable mass as a function of conductor radius for Node 7

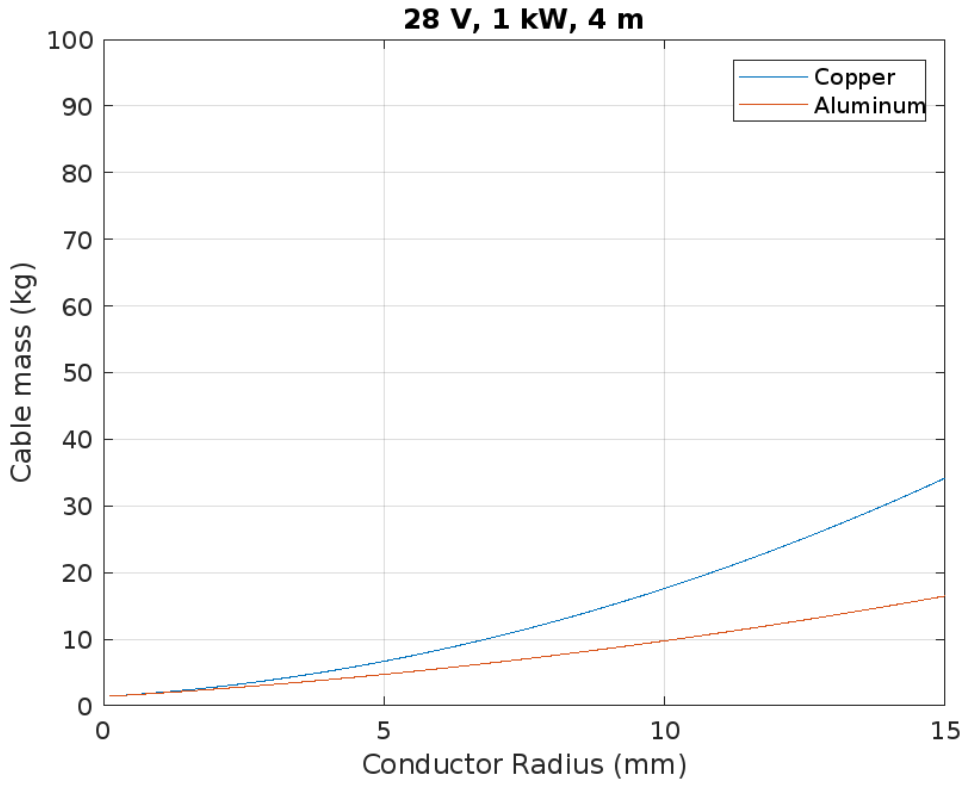

Figure A.25: Cable mass as a function of conductor radius for Node 8

A.5. Insulation Thicknesses

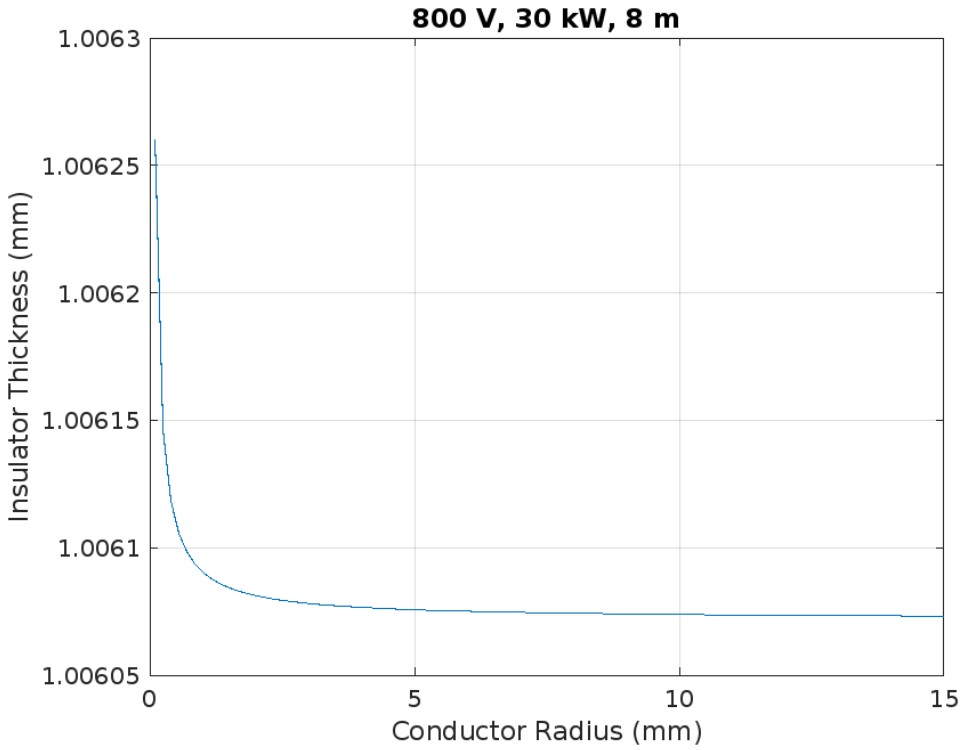

Figure A.26: Insulation thickness for nodes 3 through to 7

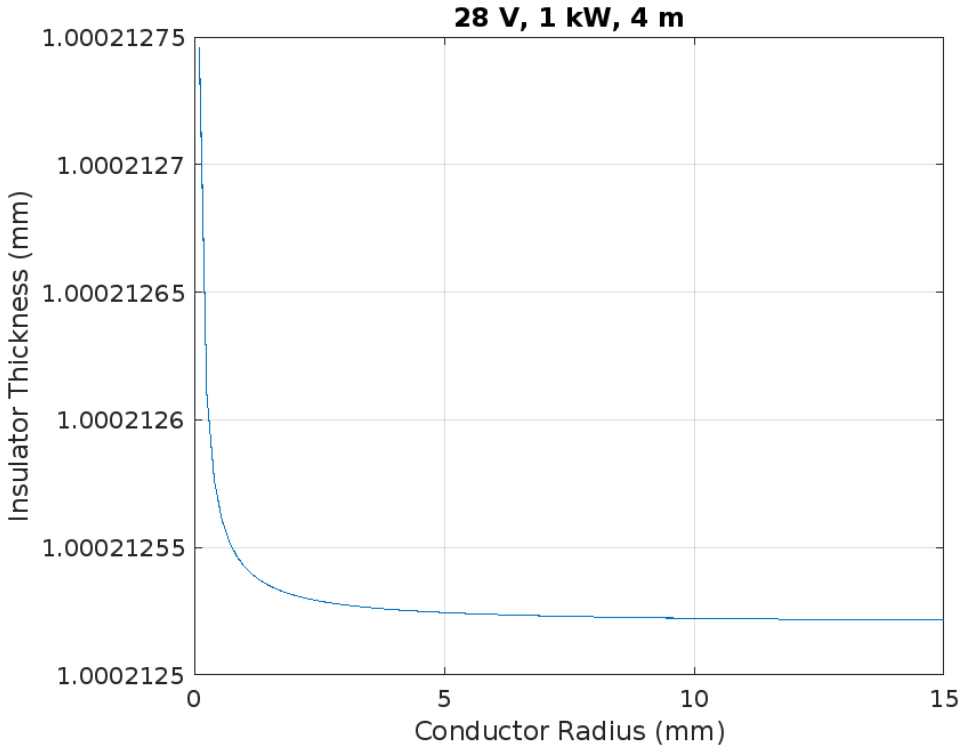

Figure A.27: Insulation thickness for node 8

B

MATLAB Code

B.1. Cable Dimension Code

```
clc
close all
V_src = 3000;
P_load = 2000e3;
length = 6;
plot_data(V_src, P_load, length, "SHIELD")

function plot_data(V_src, P_load, length, STRING)
    n = 40;
    r_c = linspace(0.1, 15, n)./1000;
    t_i = insulationThickness(r_c, V_src/2);
    V = vdrop(n, r_c, length, V_src, P_load);
    m = mass(n, r_c, t_i, length);
    temp_shield = shield_temp(V_src, r_c, t_i, length);

    if STRING == "ALL"
        figure
        plot(r_c.*1000, t_i.*1000)
        title([num2str(V_src), ' V, ', num2str(P_load/1000), ' kW, ', num2str(length), ' m'])
        xlabel('Conductor Radius (mm)')
        ylabel('Insulator Thickness (mm)')
        grid on

        T = temperature(n, r_c, t_i, V_src, P_load, length);

        figure
        plot(r_c.*1000, T);
        title([num2str(V_src), ' V, ', num2str(P_load/1000), ' kW, ', num2str(length), ' m'])
        xlabel('Conductor Radius (mm)')
        ylabel('Temperature (C)')
        legend('Copper', 'Aluminum')
        ylim([0, 250])
        grid on

        figure
        plot(r_c.*1000, 100.*V./V_src);
        title([num2str(V_src), ' V, ', num2str(P_load/1000), ' kW, ', num2str(length), ' m'])
        xlabel('Conductor Radius (mm)')
        ylabel('Line Voltage Drop (%)')
        legend('Copper', 'Aluminum')
        ylim([0, 2])
        grid on

        figure
        plot(r_c.*1000, m)
        title([num2str(V_src), ' V, ', num2str(P_load/1000), ' kW, ', num2str(length), ' m'])
        xlabel('Conductor Radius (mm)')
        ylabel('Cable mass (kg)')
```

```
        legend('Copper', 'Aluminum')
        ylim([0, 100])
        grid on

        figure
        plot(r_c.*1000, temp_shield)
        title('Shield Temperature Change')
        xlabel('Conductor Radius (mm)')
        ylabel('Temperature (C)')
        grid on

    elseif STRING ~= "TEMP"
        figure
        plot(r_c.*1000, t_i.*1000)
        title([num2str(V_src), ' V, ', num2str(P_load/1000), ' kW, ', num2str(length), ' m'])
        xlabel('Conductor Radius (mm)')
        ylabel('Insulator Thickness (mm)')
        grid on

        figure
        plot(r_c.*1000, 100.*V./V_src);
        title([num2str(V_src), ' V, ', num2str(P_load/1000), ' kW, ', num2str(length), ' m'])
        xlabel('Conductor Radius (mm)')
        ylabel('Line Voltage Drop (%)')
        legend('Copper', 'Aluminum')
        ylim([0, 2])
        grid on

        figure
        plot(r_c.*1000, m)
        title([num2str(V_src), ' V, ', num2str(P_load/1000), ' kW, ', num2str(length), ' m'])
        xlabel('Conductor Radius (mm)')
        ylabel('Cable mass (kg)')
        legend('Copper', 'Aluminum')
        ylim([0, 100])
        grid on

        figure
        plot(r_c.*1000, temp_shield)
        title('Shield Temperature Change')
        xlabel('Conductor Radius (mm)')
        ylabel('Temperature (C)')
        grid on
    else
        T = temperature(n, r_c, t_i, V_src, P_load, length);

        figure
        plot(r_c.*1000, T);
        title([num2str(V_src), ' V, ', num2str(P_load/1000), ' kW, ', num2str(length), ' m'])
        xlabel('Conductor Radius (mm)')
        ylabel('Temperature (C)')
        legend('Copper', 'Aluminum')
        ylim([0, 250])
        grid on
    end
end

function t_i = insulationThickness(r_c, V_max)
    epsilon = 2.3;
    K = 3*epsilon/(1+2*epsilon);
    alpha = 250;
    t_v = 30.8/10e6;
    C = 0.1/100;
    t_i = r_c.*(exp((K*V_max*t_v)./(alpha.*r_c))-1) + C;
end

function V = vdrop(n, r_c, length, V_max, P_load)
    I = P_load/V_max;
    Resistivity = [1.72e-8, 2.65e-8]; %ohm*m [Copper, Aluminum]
    Alpha = [0.00394, 0.00429];
    T_ref = 20;
```

```
    V = zeros(2, n);
    T_c = 250;
    for i = 1:2
        R_ref = zeros(n);
        for j = 1:n
            R_ref(j) = Resistivity(i)*length/(pi*r_c(j)^2);
            R_c = R_ref(j)*(1+Alpha(i)*(T_c-T_ref));
            V(i, j) = I*R_c;
        end
    end
end

function T = temperature(n, r_c, t_i, V_max, P_load, length)
    I = P_load/V_max;
    Resistivity = [1.72e-8, 2.65e-8]; %ohm*m [Copper, Aluminum]
    Alpha = [0.00394, 0.00429];
    t_sc = 1.2e-3;
    T_ref = 20;
    T_amb = 30;
    h = 11;
    k = 0.28;
    T = zeros(2, n);
    T_c = 90;
    for i = 1:2
        R_ref = zeros(n);
        for j = 1:n
            A = 2*length*(t_sc+t_i(j) + r_c(j))*pi;
            R_ref(j) = Resistivity(i)*length/(pi*r_c(j)^2);
            syms T_ci
            R_c = R_ref(j)*(1+Alpha(i)*(T_c-T_ref));
            eq2 = h*A*(T_ci-T_amb) == I^2*R_c;
            S = solve(eq2);
            T_i = S;
            T_1 = 1/(2*pi*k)*log(1+(t_i(j)+t_sc)/(r_c(j)));
            W_loss = I^2*R_ref(j)/length;
            delta_Theta = T_1*W_loss;
            T(i, j) = delta_Theta+T_i;
        end
        if i == 1
            disp("Halfway with calculations")
        end
    end
end

function m = mass(n, r_c, t_i, length)
    shield_density = 8960;
    t_s = 2e-3;
    insulator_density = 930;
    con_density = [8960, 2700];
    A_c = pi.*r_c.^2;
    A_i = (pi.*(2.*t_i+r_c).^2)-A_c;
    A_s = (pi.*(t_s + 2.*t_i+r_c).^2)-A_i-A_c;
    m = zeros(2, n);
    for i = 1:2
        m(i, :) = (A_c.*con_density(i).*length)+(A_i.*insulator_density.*length)...
            +(A_s.*shield_density.*length);
    end
end

function t = shield_temp(V_max, r_c, t_i, length)
    density = 8960;
    t_short = 300e-6;
    C = 385;
    t_s = 2e-3;
    A_c = pi.*r_c.^2;
    A_i = (pi.*(2.*t_i+r_c).^2)-A_c;
    A_s = (pi.*(t_s + 2.*t_i+r_c).^2)-A_i-A_c;
    R_i = 50e-3;
    I = V_max/(2*R_i);
    m = A_s.*density.*length;
    t = (t_short*R_i*I^2)./(m.*C);
```

```
191 end
```